THE JOURNAL OF PHYSICAL CHEMISTRY C

Article

pubs.acs.org/JPCC

Relationship between the Synthesis of Prussian Blue Pigments, Their Color, Physical Properties, and Their Behavior in Paint Layers

Louise Samain,*[,†,⊥] Fernande Grandjean,[‡,§] Gary J. Long,[§] Pauline Martinetto,[∥] Pierre Bordet,[∥] and David Strivay[†]

[†]European Center of Archaeometry, University of Liège, Sart Tilman B15, B-4000 Liège, Belgium

[‡]Faculty of Sciences, University of Liège, Sart Tilman B6, B-4000 Liège, Belgium

[§]Department of Chemistry, Missouri University of Science and Technology, University of Missouri, Rolla, Missouri 65409-0010, United States

[∥] Institut Néel, CNRS and Université Joseph Fourier, BP 166, F-38042 Grenoble Cedex 9, France

Supporting Information

ABSTRACT: Prussian blue pigments, highly insoluble mixed-valence iron(III) hexacyanoferrate(II) complexes of typical stoichiometry $Fe_4^{III}[Fe^{II}(CN)_6]_3{\cdot}xH_2O$ or $KFe^{III}[Fe^{II}(CN)_6]{\cdot}xH_2O$, have been used as pigments in oil paintings and watercolors for 300 years. For poorly understood reasons, these pigments often fade with time. Although the preparation methods have been recognized since the mid-eighteenth century as a contributory factor in the fading of the pigment, the spectral and physical properties of Prussian blue that vary with the type of synthesis were not precisely identified. Several Prussian blue pigments have been prepared by different methods and characterized by thermogravimetric analyses, high-energy powder X-ray diffraction, atomic absorption and flame emission, UV−visible, iron-57 Mössbauer, iron K-edge X-ray absorption, and Raman spectroscopy. The type of synthesis influences the hue, tinting strength, and hiding power properties of the Prussian blue pigments. Two major features appear to be strongly dependent on the preparative methods, the particle size and the local disorder. Both a nitrogen atmosphere and an intermediate aging step of the Berlin white, $Fe_2^{II}[Fe^{II}(CN)_6]$, during the synthesis are required to obtain a highly colored pigment through the optimization of particle size, minimization in the perturbations to the Fe^{II}−CN−Fe^{III} intervalence electron transfer pathway, and the minimization of disordered vacancies. The potassium containing Prussian blue structure has been revisited. It can be described with the *Pm*3*m* space group, where approximately one-quarter of the $[Fe^{II}(CN)_6]^{4-}$ sites are vacant and where the potassium cation is located at a zeolitic-like position inside the lattice cavities. The degree of ordering of the $[Fe^{II}(CN)_6]^{4-}$ vacancies in all Prussian blues was quantified using atomic pair distribution analysis, an ordering that is consistent with the iron K-edge X-ray absorption spectra. The presence of strain in the crystals is observed by both powder X-ray diffraction and Mössbauer spectroscopy. The structural similarity between the alkali-free, improperly referred to as "insoluble", and the alkali containing, "soluble", Prussian blues may explain why the two varieties are almost undistinguishable by spectroscopic techniques.

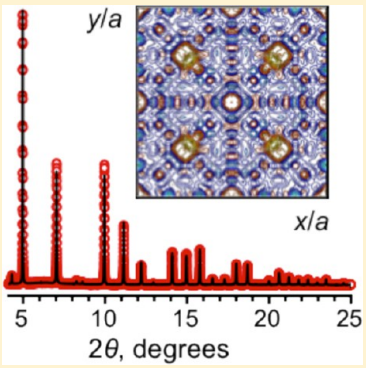

INTRODUCTION

Prussian blue has been widely used and studied since its discovery ca. 300 years ago because of its various unusual properties, for example, its intense blue color and its electrochromism,[1−3] magnetism at low temperature,[4,5] zeolitic character,[6,7] and semiconductor behavior.[8,9]

Prussian blue is known to contain a hydrated iron(III) hexacyanoferrate(II) anion, $\{Fe^{III}[Fe^{II}(CN)_6]{\cdot}xH_2O\}^-$, with varying values of x up to 16, and various cations, such as K^+, NH_4^+, or Na^+. An alkali-free Prussian blue, $Fe^{III}_4[Fe^{II}(CN)_6]_3{\cdot}xH_2O$, which must have an increased amount of iron(III) to maintain charge balance, is commonly referred to as the insoluble Prussian blue, whereas those Prussian blues containing alkali cations are referred to as the soluble Prussian blues. Even though all Prussian blues are highly insoluble, with a solubility product of ca. 1×10^{-41}, the soluble appellation refers to those Prussian blues that are easily dispersed in an aqueous solution to form a colloidal suspension. Although perhaps unfortunate, the widely used historical soluble and insoluble designation will be used herein. The blue color of Prussian blue is produced by an intervalent electron transfer[10] from an iron(II) to an iron(III) ion in different local atomic environments when light is absorbed at ca. 700 nm.

Because of its composition, Prussian blue is considered as the prototype of mixed valence compounds and of cubic polynuclear transition-metal cyanide complexes.[11] These transition-metal cyanide complexes are characterized by an open framework structure and an inherent structural disorder,[12] two features that

Received: November 10, 2012
Revised: March 19, 2013
Published: April 11, 2013

   dx.doi.org/10.1021/jp3111327 | *J. Phys. Chem. C* 2013, 117, 9693−9712

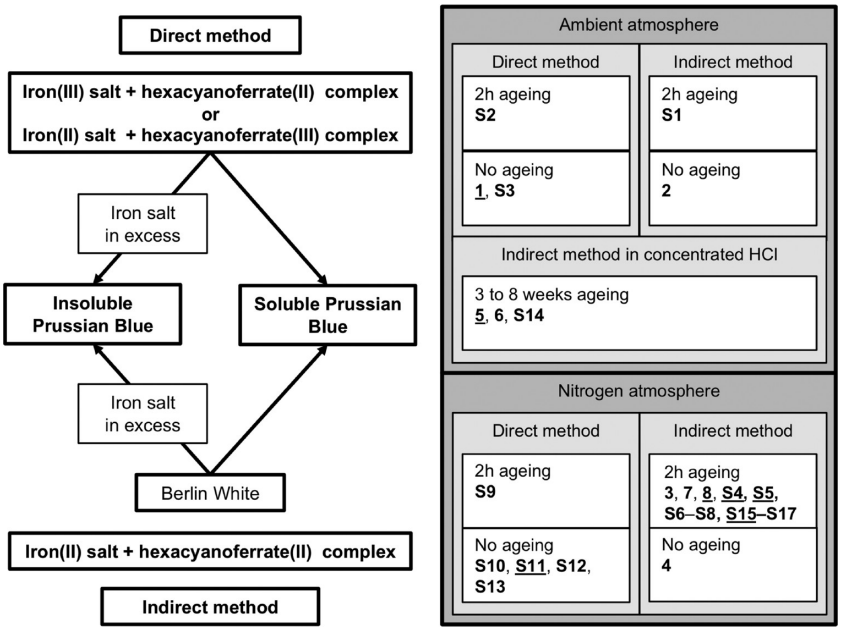

Figure 1. Schematic representation of the direct and indirect methods used to produce modern Prussian blue pigments (left) and classification of all of the Prussian blue pigments reported in this work according to their synthesis routes (right). The underlined pigments are insoluble Prussian blues, whereas the others are soluble Prussian blues.

make their analytical and structural characterization rather problematic.

Although Prussian blue has been known for more than 300 years, many problems related to its crystal structure and fading behavior in paint layers remain unsolved. First, Prussian blue pigments often irreversibly fade when used in paint layers. The preparation methods of Prussian blue have been recognized as a contributory factor in the fading of the pigment, but, to date, no satisfactory explanation for this alteration is known.[13,14] A better understanding of the mechanisms associated with this degradation is of primary importance in the preventive conservation and restoration of paintings in which Prussian blue pigments have been used. Second, confusion exists over the distinction between the "soluble" and the "insoluble" varieties of Prussian blue pigments. Third, the crystal structure of soluble Prussian blue is still open to debate. The commonly accepted structural model of soluble Prussian blue that was proposed by Keggin and Miles[15] in 1936 has been recently revisited.[16] In particular, the location of the water molecules and the alkali cation and the quantification of the local disorder in the soluble variety remain unclear. These points cannot be clarified without investigating the preparation conditions of Prussian blue.

The synthesis of Prussian blue is based on a precipitation reaction between an iron salt and an alkali hexacyanoferrate. Prior to the mid-nineteenth century, the alkali hexacyanoferrate could not be produced in bulk because of limited chemical knowledge. Thus, before the mid-nineteenth century, the essential alkali hexacyanoferrate starting reagent was indirectly produced[17] by calcination of animal matter with an alkali. A related paper[18] is devoted to the synthesis and study of the fading of eighteenth-century Prussian blue pigments. By the mid-nineteenth century, it was discovered that potassium hexacyanoferrate could be extracted from gas purification products.[19] This discovery marks the beginning and the commercialization of the so-called modern methods for producing Prussian blue, methods that are completely inorganic in nature in contrast to the eighteenth-century methods that used an organic starting material.

Herein, the modern preparative methods of bulk Prussian blue are reviewed and reproduced to identify the spectral and physical properties that vary with the type of synthesis. The disorder, the differences between the soluble and insoluble Prussian blues, and their behavior in paint layers have been investigated through a detailed analytical and structural characterization of the Prussian blues with the long-term goal of better understanding the physical basis for their fading over time. The degradation mechanisms associated with this fading effect have been investigated in two related papers.[18,20]

EXPERIMENTAL SECTION

Synthesis. The modern methods for the production of Prussian blue pigments are based on the precipitation reaction between an iron salt and a hexacyanoferrate complex and are of two types, direct and indirect; see Figure 1.

The direct method of preparing Prussian blue is a one-step process and consists of mixing a solution of an iron(III) salt with a solution of a hexacyanoferrate(II) salt. The deep blue precipitate is filtered and carefully washed with distilled water. Alternatively, a mixture of solutions of an iron(II) salt and a hexacyanoferrate(III) salt produces the so-called Turnbull's blue considered to be a ferrous ferricyanide. In the 1960s, Mössbauer spectroscopy and X-ray diffraction revealed that both reactions yield the same compound,[5,21] that is, iron(III) hexacyanoferrate-(II). If the iron salt is present in excess, the precipitate is the insoluble Prussian blue pigment, typically $Fe_4^{III}[Fe^{II}(CN)_6]_3 \cdot xH_2O$, whereas if the reagents are mixed in a 1:1 molar ratio or with the hexacyanoferrate present in excess, a soluble Prussian blue pigment, typically $KFe^{III}[Fe^{II}(CN)_6] \cdot xH_2O$, results.

The indirect method is the most commonly used preparative method in the pigment industry, which currently produces[22] ca. 10^7 kg per year. It is a two-step process based on the reaction between an iron(II) salt and a hexacyanoferrate(II) salt. From

dx.doi.org/10.1021/jp3111327 | J. Phys. Chem. C 2013, 117, 9693−9712

Table 1. Mössbauer Spectral Parameters of the Prussian Blue Pigments[a]

expected composition	δ^{II}, mm/s[b]	$\Delta E_Q{}^{II}$, mm/s	Γ^{II}, mm/s	A^{II},[c] %	δ^{III}, mm/s[b]	$\Delta E_Q{}^{III}$, mm/s	Γ^{III}, mm/s
$Fe_4^{III}[Fe^{II}(CN)_6]_3{\cdot}xH_2O$ (**1**)	−0.146(1)	0.110(6)	0.263(7)	43(1)	0.400(5)	0.530(6)	0.466(9)
$NH_4Fe^{III}[Fe^{II}(CN)_6]{\cdot}xH_2O$ (**2**)	−0.132(2)	0.07(2)	0.33(1)	48(1)	0.435(7)	0.30(1)	0.57(2)
$KFe^{III}[Fe^{II}(CN)_6]{\cdot}xH_2O$ (**3**)	−0.140(1)	0.042(1)	0.237(1)	47(1)	0.400(1)	0.000(5)	0.400(1)
$KFe^{III}[Fe^{II}(CN)_6]{\cdot}xH_2O$ (**4**)	−0.141(1)	0.06(1)	0.294(5)	45(1)	0.404(3)	0.340(4)	0.52(1)
$KFe^{III}[Fe^{II}(CN)_6]{\cdot}xH_2O$ (**7**)[d]	−0.138(1)	0.076(8)	0.251(7)	48(1)	0.404(2)	0.07(3)	0.40(1)
$Fe_4^{III}[Fe^{II}(CN)_6]_3{\cdot}xH_2O$ (**8**)[d]	−0.141(1)	0.114(4)	0.247(6)	46(1)	0.408(3)	0.230(5)	0.41(1)

[a]Statistical errors are reported; more realistic errors are ±0.005 mm/s for the isomer shifts, δ, and ±0.01 mm/s for the quadrupole splittings, ΔE_Q, and line widths, Γ. [b]The isomer shift, δ, is referred to α-iron powder at 295 K. [c]A^{II} is the percent area of the iron(II) doublet and $A^{III} = 100 - A^{II}$. [d]The exact compositions of **7** and **8** have been determined from Rietveld refinement of powder X-ray diffraction patterns; see below.

the solution a precipitate of the so-called Berlin white, the ferrous ferrocyanide, $Fe_2^{II}[Fe^{II}(CN)_6]$, is obtained, a precipitate that is then treated with a powerful oxidizing agent such as hydrogen peroxide, or an alkali metal chlorate or chromate, to yield Prussian blue. Again, depending on the starting reagent that is in excess, the soluble or insoluble Prussian blue is obtained.

Three types of modern syntheses may be distinguished: the synthesis of bulk Prussian blue reported in scientific papers, the synthesis used by the pigment industry and described in patents, and the synthesis of well-crystallized Prussian blue.

From the literature and from patents, the parameters that apparently influence the properties of a Prussian blue pigment, such as its "apparent" solubility, color shade, or particle size, have been identified; see the Supporting Information for details. These parameters are the nature and the relative proportion of the starting reagents, the atmosphere, the rate of formation of the intermediate Berlin white, and the aging of the precipitate before oxidation. Syntheses of Prussian blue pigments were thus carried out by varying these parameters. The general procedure is detailed below. A blue precipitate was successfully obtained in all attempted syntheses. Unless otherwise stated, all reagents used herein for the synthesis of Prussian blue were of reagent grade and obtained from Sigma-Aldrich, Steinheim, Germany.

The starting reagents were dissolved in deionized water in the appropriate relative concentration. They were mixed together under magnetic stirring. In case of an indirect process, Berlin white was formed and aged for 2 h at 90 °C. Before oxidation the solution was acidified by adding hydrochloric acid. An excess of hydrogen peroxide was added to accelerate and complete the oxidation of Berlin white into Prussian blue. Filtration was difficult to achieve because of the tendency of Prussian blue to form colloidal solutions, and thus centrifugation was preferred to filtration. The precipitate was thoroughly washed with deionized water and collected by centrifugation. The pigment was oven-dried at ca. 55 °C for 1 h and then ground into a fine powder.

Details of the syntheses of samples **1**−**8** are given in Table S1 along with the entire list of the additional Prussian blue pigments that have been prepared but not reported on in detail herein. The specific "expected" stoichiometries of **1**−**4**, **7**, and **8** are given in the first column of Table 1.

The syntheses of **1**−**4** produce Prussian blue as a fine colloidal precipitate. This colloidal nature of Prussian blue pigments has been a major difficulty in determining the exact composition and the crystal structure of Prussian blue pigments. In 1977, Buser et al.[23] succeeded in growing Prussian blue single-crystals. They prepared a solution of iron(II) and $[Fe^{II}(CN)_6]^{4-}$ in concentrated hydrochloric acid and allowed crystals to grow by very slow diffusion of water vapor into the solution. After 8 weeks they collected cubic crystals as large as 0.15 mm in length. The Buser et al.[23] synthesis has been reproduced here and was adapted to produce both the insoluble well-crystallized Prussian blue, $Fe_4^{III}[Fe^{II}(CN)_6]_3{\cdot}xH_2O$, **5**, and the soluble well-crystallized Prussian blue, $NH_4Fe^{III}[Fe^{II}(CN)_6]{\cdot}xH_2O$, **6**.

Insoluble crystallized Prussian blue, **5**, see Table S1, was prepared by separately dissolving 7.5 mmol of $FeCl_2{\cdot}4H_2O$ and 2.5 mmol of $K_4Fe(CN)_6{\cdot}3H_2O$ in 35 mL of deionized water. The two solutions were added to 430 mL of 36% HCl to obtain 500 mL of a solution containing 10 mol/L of HCl. The beaker containing this solution and another beaker containing ca. 500 mL of water were both placed in a vacuum desiccator whose stopcock was open. The diffusion of air into the solution slowly oxidizes the iron(II) ions. After 8 weeks in the dark, cubic crystals of **5** were collected by filtration, thoroughly washed with 2 M HCl, 0.1 M HCl, and finally with deionized water, until the absence of turbidity was observed upon addition of $AgNO_3$ to the wash water.

The procedure used to prepare soluble well-crystallized Prussian blue, **6**, containing NH_4^+ ions is identical to that for insoluble Prussian blue, **5**, except for the proportion of starting reagents. Equimolar quantities, 5.0 mmol of $FeCl_2{\cdot}4H_2O$ and 5.0 mmol of $(NH_4)_4Fe(CN)_6{\cdot}xH_2O$, obtained from Fluka with a purity of at least 85%, were used. In this case, 3 weeks was required to obtain large cubic crystals of **6**.

Commercial Prussian blue pigments, **7** and **8**, have been obtained to compare their properties with those of **1**−**6** prepared herein. A commercial soluble Prussian blue pigment, with an undefined but probable stoichiometry of $KFe^{III}[Fe^{II}(CN)_6]{\cdot}xH_2O$, **7**, manufactured prior to 1948 by Winsor and Newton, London, was provided by the Royal Institute for Cultural Heritage, Brussels, Belgium. The insoluble Prussian blue, $Fe_4^{III}[Fe^{II}(CN)_6]_3{\cdot}xH_2O$, **8**, was purchased from Sigma Aldrich, Steinheim, Germany.

In total, 20 Prussian blue pigments, including three well-crystallized pigments, and five commercial pigments were available for analyses; see Table S1. With the goal of identifying the role that the various synthesis parameters play upon the properties of Prussian blue pigments, the detailed characterization of the selected samples, **1**−**8**, is reported herein. More details of the remaining samples may be found in the Supporting Information and in ref 24.

UV−Visible Spectroscopy. UV−visible absorption spectra were obtained between 350 and 900 nm in a quartz cell by using a Kontron Uvikon 941 double-beam spectrophotometer. Prussian blue colloidal solutions were prepared by dispersing 1 mg of Prussian blue pigment in 10 mL of deionized water. To obtain as fine as possible dispersions of the pigments, the blue colloidal suspensions were sonicated for 15 min in an ultrasonic bath. This process led to "solutions" that exhibited no visual scattering for the soluble pigments, **3** and **4**, but was less successful for the insoluble pigment **8**.

dx.doi.org/10.1021/jp3111327 | J. Phys. Chem. C 2013, 117, 9693−9712

The UV−visible reflectance spectra were obtained with a StellarNet EPP2000C spectrometer equipped with a charge-coupled detector. The optical-fiber probe consists of six illuminating fibers and a single fiber that collects the reflected light. The sample is illuminated over a surface area of ca. 4 mm^2 at an angle of 45° to avoid direct reflection. A Halon D50 white lamp reference was used for calibration. The spectra were recorded in reflection mode between 350 and 880 nm, with a resolution of 1 nm.

Scanning Electron Microscopy. The scanning electron microscopy measurements were obtained with a JEOL JSM-7500F field-emission electronic scanning microscope. The scanning electron micrographs were obtained with an emission current of 10 μA and a 15 keV electron beam. The micrographs were recorded in the secondary electron emission mode; the contrast is thus related to the topography of the sample surface. Powder Prussian blue samples were deposited on a double-sided carbon tape on the sample holder and introduced in the microscope. Because of the semiconducting behavior of Prussian blue, no sample charging was observed during the measurements.

Nitrogen Adsorption−Desorption. The nitrogen adsorption−desorption isotherms of selected Prussian blues have been recorded using a Sorptomatic 1900 Fisons instrument. The specific surface area was determined by using the Brunauer−Emmett−Teller theory.

Iron-57 Mössbauer Spectroscopy. Iron-57 Mössbauer spectra were obtained by using a constant-acceleration spectrometer and a Janis Supervaritemp cryostat. The Mössbauer spectral absorbers were prepared with 10 mg/cm^2 of powdered Prussian blue pigment mixed with boron nitride. The spectrometer was calibrated at 295 K with α-iron powder. The Mössbauer spectra were fitted with Lorentzian symmetric doublets from 7 to 295 K or with a doublet and a sextet at 4.2 K.

Atomic Absorption and Flame Emission Spectroscopy. The Prussian blue pigments were dissolved in concentrated sulfuric acid and then treated with hydrochloric acid to dissolve the iron sulfate formed. The concentrations of iron and potassium are given in weight percent and are the average of three successive measurements. The accuracy of the measurement is estimated to be ±0.01 wt %.

Thermogravimetric Analyses. Thermogravimetric analyses, coupled with differential thermal analyses, were obtained with a Netzsch STA 447 C instrument. The Prussian blue pigments were placed in an alumina crucible and heated with a constant heating rate of 2 °C/min in air. The thermogravimetric curves were normalized, that is, divided by the sample mass, so that they begin at 100%.

Particle-Induced X-ray Emission Spectroscopy. The particle-induced X-ray emission measurements were performed by using an external proton beam of ca. 3.12 MeV with an intensity of 5 nA, produced by the cyclotron of the University of Liège. Description and recent improvements of the PIXE line and extraction nozzle have been described by Weber et al.[25] The specific experimental conditions and the fitting procedure are detailed in the Supporting Information.

The spectra were analyzed with the GUPIXWIN software.[26] Calibration in energy and adjustment of the experimental parameters were achieved by fitting a diorite, DR-N, standard. Prussian blue powders were analyzed in the form of pressed pellets and were considered as thick targets. The elemental composition was calculated by taking into account the invisible elements, that is, the light elements that are known to be present in the sample but whose X-rays are not detected, such as C and N; see Supporting Information for details. The water was not considered in the elemental composition.

X-ray Diffraction. The Prussian blue pigments were studied by X-ray powder diffraction with a PANalytical PW-3710 diffractometer. The radiation was provided by an iron anode that produced iron K_α radiation of 1.9373 Å wavelength. The use of iron radiation reduces the fluorescence of the sample, because iron is the main constituent of Prussian blue. Unless otherwise stated, the diffraction patterns were recorded over a 2θ angle range from 5° to 75°, with a time per step of 1 s.

The high-energy X-ray diffraction experiments were carried out at the beamline ID11, European Synchrotron Radiation Facility (ESRF), Grenoble. This beamline is equipped with a Si(111) double crystal monochromator and a X-ray transfocator. The beam size was approximately 50 × 200 μm^2 area. The X-ray energy was 99.428 keV, and the wavelength is 0.124968 Å. The Prussian blue pigments were stored in quartz capillaries of 0.3 mm in diameter and placed in front of the detector. A total of 81 2D diffraction images per sample, with an acquisition time of 20 s per image, were collected with the ESRF FreLoN camera placed at ca. 107 mm from the sample. The 2D diffraction images were then averaged and integrated into a linear scattering signal with the software Fit2D.[27] The distance between the sample and the detector was determined with a LaB_6 standard.

According to the formalism developed by Proffen and Billinge,[28] the pair distribution function, $G(r)$, may be obtained from the powder X-ray diffraction pattern by a Fourier transform of the normalized scattering intensity, $S(Q)$, which contains the coherent scattering intensity; see the Supporting Information for details.

$$G(r) = 4\pi r[\rho(r) - \rho_0] = \frac{2}{\pi}\int_0^\infty Q[S(Q) - 1]\sin Qr\, dQ \quad (1)$$

where $\rho(r)$ is the microscopic pair density, ρ_0 is the atomic number density, that is, the number of electrons per $Å^3$, and Q is the magnitude of the scattering vector. For elastic scattering $Q = 4\pi \sin\theta/\lambda$, where 2θ is the scattering angle and λ the wavelength of the radiation used. The function $G(r)$ in eq 1, which is referred to as the reduced pair distribution function, gives the probability of finding an atom or ion at a distance, r, from any given atom or ion.

The pair distribution function is extracted by using the PDFgetX2 software.[29] The pair distribution function was obtained by using a Gaussian damping of 15−20 $Å^{-1}$, and a maximum Q-value, Q_{max}, of 30 $Å^{-1}$. Details of this extraction are given in the Supporting Information.

The software PDFGui[30] was used for the pair distribution function refinement. The refinement is based on the least-squares minimization in direct space of the experimental pair distribution with a structural periodic model; see the Supporting Information for details. In the pair distribution function analysis of the Prussian blue pigments, the lattice parameter, a, the scale factor for each phase, and the position, the occupancy, and isotropic atomic displacement parameters for each atom or ion in each phase were refined up to a maximum distance, herein fixed at 10.2 Å, that is, ca. the lattice parameter of Prussian blue. The resolution damping factor accounts for the progressive decrease in the amplitude of the pair distribution function peaks at larger distances due to the resolution of the diffraction experiment. This factor was determined to be 0.05 from the LaB_6 standard pair distribution analysis. This value was used in all of the fits

dx.doi.org/10.1021/jp3111327 | J. Phys. Chem. C 2013, 117, 9693−9712

presented herein as the data were recorded under similar experimental conditions.

The high-resolution X-ray powder diffraction data used for the Rietveld refinement were collected at the CRISTAL beamline, Soleil, Paris. The beamline is located at an undulator port and provides a beam in the energy range of 4−30 keV, with a relative energy resolution, $\Delta E/E$, of approximately 10^{-4}. The beam cross-section on the sample is ca. 450 × 100 μm^2. The X-ray powder diffraction data were collected at a wavelength of 0.442930 Å in high resolution, parallel beam geometry using a multianalyzer/detector stage. The samples were placed in 0.7 mm diameter glass capillaries. The data were refined by the Rietveld method using the FULLPROF software.[31]

Iron K-Edge X-ray Absorption Spectroscopy. The iron K-edge X-ray absorption near-edge experiments were performed at the DUBBLE Dutch-Belgian beamline BM26, which is located at a 0.4 T bending magnet port of the electron storage ring, at the ESRF, Grenoble, France. This beamline,[32] which is equipped with a Si(111) double crystal monochromator, delivers an X-ray beam with an energy of 9.6 keV and a relative energy resolution, $\Delta E/E$, of ca. 2×10^{-4}. The higher harmonics were suppressed with a silicon reflecting strip on a mirror behind the monochromator.

The energy scale was calibrated with a 4 μm thick iron foil, whose spectrum was recorded in transmission mode; the energy of the first maximum in the derivative of the absorption at the iron K-edge was taken to be 7112 eV. In transmission mode, the intensities of the incident and transmitted X-ray beams were measured with Oxford Instrument ionization detectors. Ground mixtures of Prussian blue pigments with boron nitride were pressed into self-supporting pellets and then measured in transmission mode.

The X-ray absorption near-edge spectral data reduction and analysis were performed with the XDAP software.[33] A modified Victoreen curve[34] was used for the pre-edge background subtraction in the X-ray absorption spectra obtained in transmission mode, and a linear function or a constant was used for the same subtraction in the spectra obtained in fluorescence detection mode. A cubic spline routine[35] was used for the atomic background subtraction. The pre-edge background subtracted spectra were normalized to the edge height, which was taken to be the value of the atomic background at 50 eV above the K-edge. The fit parameters were determined by multiple shell fitting in *R*-space, by applying the difference file technique using Fourier transforms.[36] The phase shifts and backscattering amplitudes were obtained form FEFF8.0 calculations[37] on the Prussian blue crystal structure, by taking the iron(II) ion as the central ion site. Details about the fit procedure used herein can be found elsewhere.[14]

Raman Spectroscopy. The Prussian blue powders were studied by using a Horiba Jobin Yvon LabRAM 300 Raman spectrometer that used either a Krypton ion laser at a wavelength of 647 nm, which enhances the band intensities of Prussian blue by resonance Raman effects, or an Ar laser at a wavelength of 514 nm with a power of 0.3 mW. All spectra are the result of the sum of two scans with an integration time of 100 s between 2800 and 100 cm^{-1}; the resolution is 5 cm^{-1}. The baseline of the Raman spectra was corrected with a polynomial function.

RESULTS

Our long-range goal is the study of the causes of fading of Prussian blue pigments in eighteenth- and nineteenth-century paintings, and the main objective of this article is to investigate the Prussian blue synthesis−properties relationship. Our starting point is the characterization of the color of Prussian blue pigments painted both pure and mixed with a white pigment because the color is the key property for the study of any subsequent fading. Because of the well-known dependence of the color properties on the intrinsic grain size distribution, the particle size of the pigments has been determined and related to the color characteristics. The color of Prussian blue arises from the presence of the $Fe^{II}-CN-Fe^{III}$ exchange pathway, which allows intervalent electron transfer when light is absorbed at approximately 700 nm. Any subsequent color change is thus related to this specific structural pathway, which is extensively studied herein by X-ray diffraction, pair distribution function analysis, and iron K-edge absorption spectroscopy. Prior to this thorough structural characterization, the composition of the Prussian blue pigments has been carefully investigated. Mössbauer spectroscopy has been used to identify the ferric ferrocyanide complex and determine the iron(III)/iron(II) ratio. The elemental composition of the Prussian blue pigments was obtained by combining atomic thermogravimetric analyses, atomic absorption and flame emission spectroscopy, and particle-induced X-ray emission studies. As will be shown below, the iron(III)/iron(II) ratio obtained from Mössbauer spectroscopy and the elemental composition do not agree with the usual stoichiometry for soluble potassium containing Prussian blue, that is, $KFe^{III}[Fe^{II}(CN)_6]\cdot xH_2O$, and a new structural model derived from the Rietveld refinement of a high-resolution X-ray powder diffraction pattern is proposed to resolve these discrepancies.

Color, Spectral Reflectance, and Absorbance. Both because of the importance of Prussian blue as an artist's pigment and because of its tendency to fade with time, its color must be carefully evaluated to better delineate future painting conservation and restoration methods.

In Figure 2, the different Prussian blue pigments mixed with gum arabic have been painted in a pure state or mixed with 100 parts of titanium white, TiO_2, a modern white pigment purchased from Kremer Pigmente Gmbh & Co. KG, Alchstetten, Germany. Although the commercial and laboratory-synthesized Prussian blue pigments are all qualitatively blue in color, it is visually obvious in Figure 2 that the color is not identical for all of the pigments painted either pure or mixed with TiO_2.

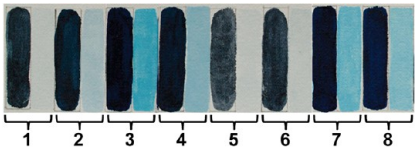

Figure 2. Paint layers of Prussian blue pigments, **1**−**8**, mixed with gum arabic and painted pure, left of each pair, and mixed with 100 parts of TiO_2, right of each pair.

The color of a pigmented paint layer is best evaluated in terms of three parameters. First is the hue or shade, that is, the property of a color that differentiates it from an achromatic color such as gray or black.[38] Second is the tinting strength, which is defined as the ability of a pigment to color a white mixture.[38] Third is the hiding power, a parameter that refers to the ability of a pigment to scatter light to the maximum possible extent.[39]

Several of the Prussian blue pigments, **1**, **2**, **5**, and **6**, and, to a lesser extent, **4**, are characterized by a duller shade, a lower tinting strength, and a smaller hiding power than **3** and the commercial

dx.doi.org/10.1021/jp3111327 | J. Phys. Chem. C 2013, 117, 9693−9712

pigments, **7** and **8**. These tinctorial properties are directly associated with the absorption and scattering power of the pigments, the refractive indices of the pigments and the gum arabic medium, the particle size and shape of the pigments, and their distribution.

Prussian Blue Hue. The hue of a pigment is influenced by its absorption of light, that is, by the possible electronic transitions within the molecules making up the pigment. The color of Prussian blue pigments results from an intervalence electron transfer absorption band at ca. 700 nm that corresponds to the transfer of an electron from an iron(II) to an iron(III) ion when light is absorbed.

UV−visible absorption spectral studies of aqueous dispersions of Prussian blue pigments confirm this absorption of light; see Figure 3. As expected for Prussian blue, the maxima in the

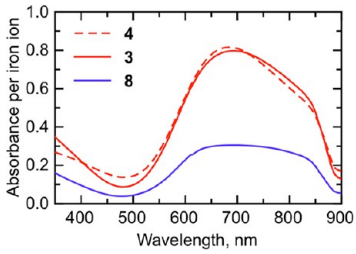

Figure 3. UV−visible absorption spectra of the soluble pigments, **3** and **4**, and the insoluble pigment, **8**.

absorbance are at 693(2), 678(2), and 692(2) nm for **3**, **4**, and **8**, respectively. A tentative fit of this UV−visible absorption spectrum is presented in the Supporting Information; see Figure S1.

The alkali metal ions present in the soluble Prussian blues also affect the hue of the pigment;[40] that is, a sodium cation containing Prussian blue is slightly greenish, whereas an ammonium cation containing Prussian blue is red-tinged. This variation in color is caused by the spectral lines of the alkali ion; a sodium ion is characterized by yellow spectral lines, a potassium ion by violet, and an ammonium cation by intense violet lines.

Analyses of the UV−visible diffuse reflectance spectra of pigments **1** and **2** painted from gum arabic with TiO_2 in a 1:100 dilution ratio revealed a shift of the maximum in reflectance toward longer wavelengths. The results are shown in Figure S2. Such a change in shade may be caused by a smaller pigment particle size.[38] The particle size of the Prussian blue pigments has been investigated by scanning electron microscopy and **4** has the smallest particle size; see Figure 4. At high magnification, the primary particles of the pigments, defined as the smallest entities that can be distinguished, can be identified; some of them are circled as a guide to the eye in the micrographs on the right in Figure 4. In the well-crystallized pigments **5** and **6**, the primary particles are cubic crystals of ca. 5 μm length. In the other pigments, the primary particles most often consist of aggregates of several crystallites. The primary particles can in turn aggregate as a result of van der Waals or Coulombic forces to form agglomerates.

All of the Prussian blue pigments studied herein as fine precipitates have formed rather shapeless agglomerates, except for the commercial pigment **8**, whose agglomerates are spherical. The commercial **S15** and **S17** Prussian blues, not shown in Figure 4, also consist of spherical agglomerates. The method for obtaining such uniform spherically shaped and lightly agglomerated particles has been described in several patents.[41] This method requires the simultaneous and very slow introduction of the aqueous solution of ferrocyanide and ferrous solution into a container with optimum mixing during the precipitation. The resulting Berlin white precipitate is then aged at temperatures between 80 and 120 °C, at a nitrogen pressure of 1−2 atm.

To complete the particle size investigation, the specific surface area of **1**, **8**, and **S15** has been measured by nitrogen adsorption−desorption. The commercial pigments **8** and **S15** have very similar specific surface areas of 55 and 61 m^2/g, whereas **1** has a specific surface area of 201 m^2/g. Because dinitrogen cannot penetrate into the lattice cavities of the Prussian blue pigments, these specific surface areas correspond to the total particle surface areas. The above values cannot be compared directly to, for instance, the BET surface area of 550 m^2/g obtained[42] for dehydrated $Fe_4^{III}[Fe^{II}(CN)_6]_3$ to probe its porosity. Thus, the specific surface area measurements confirm the smaller particle size characteristic of **1** that has been prepared in an ambient atmosphere with no aging before or during the synthesis. This smaller particle size may explain the shift in shade observed for **1** because the presence of small particles favors absorption in a wavelength region other than that of the maximum absorption observed at ca. 700 nm for Prussian blue pigments; see the Supporting Information for more details.

Tinting Strength. The shift in shade is not the most striking feature in Figure 2. The commercial pigments **7** and **8** as well as **3** are much more efficient in coloring titanium white than the other pigments. The ability of a pigment to confer color to a light scattering material is called its tinting strength. In practice, the determination of the tinting strength is based on the measurement of the reflectance corrected by the Kubelka−Munk theory.[43] This theory predicts that the tinting strength depends both on the particle size and on the wavelength of the light.

According to the Mie theory,[44] there is an optimum particle size for the absorption of light. Commercial pigments **7** and **8**, as well as **3**, have a very high tinting strength; only 1 wt % of the pigment is sufficient to color TiO_2. In contrast, the well-crystallized Prussian blue pigment **5** has an extremely low tinting strength as a result of the presence of much larger primary particles of ca. 5 μm length; see Figure 4. These larger particles are not easily penetrated by the light, and their cores remain ineffective for absorption.

Normally a reduction in particle size is expected to increase the tinting strength because additional pigment volume is accessible for absorption. However, in the case of Prussian blue pigments **1** and **2**, the smaller than optimum particle size does not enhance the tinting strength, because the light passes through the particles without absorption.

Hiding Power. The hiding power of a paint layer is related to both the absorption and scattering coefficients and the refractive indices of the pigment and the medium. The refractive index of the Prussian blue, titanium white (rutile), and gum arabic solution 10% is 1.56, 2.71, and 1.334, respectively.[45] In paint layers, the larger is the difference in refractive index between the pigment and the binder, whose refractive index is taken as 1, the higher is the hiding power because light scattering is enhanced by this large difference. With its very large refractive index and, consequently, its large scattering coefficient, titanium white is more hiding than Prussian blue, which can be considered as a transparent pigment because of its small refractive index; see Figure S3 and the Supporting Information for details. The hiding power is also influenced by the surface roughness and optical discontinuities in the paint layer.

dx.doi.org/10.1021/jp3111327 | J. Phys. Chem. C 2013, 117, 9693−9712

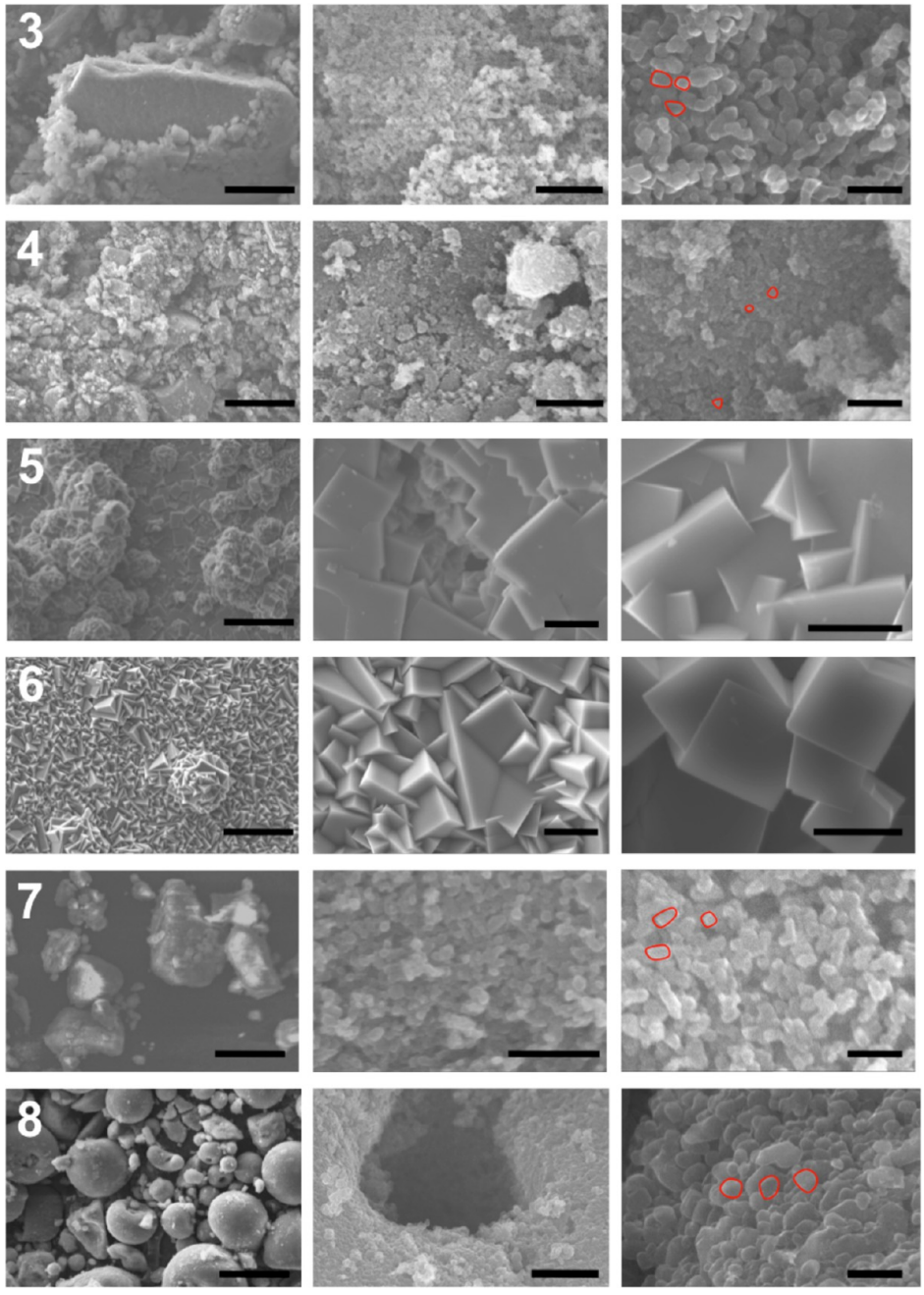

Figure 4. Scanning electron micrographs of the **3**−**8** Prussian blue pigments obtained with 15 keV secondary electrons. The scale bar is 50 μm, 1 μm, and 200 nm from left to right, except for the micrographs of pigments **5** and **6**, where the scale bar is 50, 10, and 5 μm.

As was the case for absorption, there is an optimum particle size for scattering. Unfortunately, for a given wavelength, the optimum particle size for scattering does not correspond to the optimum particle size for absorption. The scattering power reaches a maximum when the particle diameter is ca. one-half the wavelength of the incident light.[38]

Because the commercial **7** and **8**, as well as the **3** pigments are composed of particles of ca. 60−80 nm diameter, their particle size lies below the optimum size for scattering. These pigments thus have a relatively low scattering power. In contrast, **1**, **2**, and **4** are characterized by a size of ca. 20−30 nm. For particles much smaller than the wavelength of the incident light, the scattering power is better described by Rayleigh scattering than by Mie scattering. Thus, their scattering power is even weaker than that of the commercial pigments **7** and **8**, as well as that of **3**. As a pure shade they thus appear more transparent because of their small scattering power and, consequently, their poor hiding power; see Figure 2. Thus a variation in particle size explains the difference in color perception of the different Prussian blue pigments.

From Figures 2 and 4, it is obvious that the well-crystallized **5** and **6** pigments strongly differ from the **1**−**4**, **7**, and **8** pigments because of their well-crystallized character and their extremely low tinting strength. Such samples cannot be properly called pigment, which is most typically a fine coloring powder of organic or inorganic material. Because the main objective of this article is to clarify the relationship between the synthesis of Prussian blue pigments used for artistic purposes and their physical properties, **5** and **6** will not be discussed any further.

dx.doi.org/10.1021/jp3111327 | *J. Phys. Chem. C* 2013, 117, 9693−9712

In conclusion, our rather qualitative study of the color of various Prussian blue pigments indicates that the synthesis procedure strongly affects the hue, tinting strength, and hiding power of Prussian blue. Only the pigments prepared by the indirect method both in a nitrogen atmosphere and with an intermediate aging step of the Berlin white exhibit the optimum particle size to obtain a highly colored pigment.

Iron-57 Mössbauer Spectra. Iron-57 Mössbauer spectroscopy has been used to confirm both the formation and the electronic properties of the Prussian blue pigments. The Mössbauer spectra of **1**−**4**, **7**, and **8**, obtained at 295 K, are shown in Figure 5. All of the spectra have been fit with two

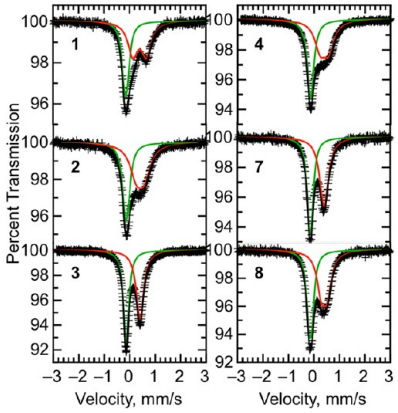

Figure 5. The 295 K Mössbauer spectra of Prussian blue pigments, **1**−**4**, **7**, and **8**. The green and red solid lines represent the low-spin iron(II) and high-spin iron(III) spectral components, respectively.

quadrupole doublets with Lorentzian lines. In some of these fits, see Table 1, the quadrupole splitting, ΔE_Q, of a doublet has become very small, even smaller than the minimum iron-57 spectral line width of 0.195 mm/s. For these doublets, the small quadrupole splittings reported in Table 1 represent the upper bound of any quadrupole splitting. The resulting isomer shifts, δ^{II} and δ^{III}, quadrupole splittings, $\Delta E_Q{}^{II}$ and $\Delta E_Q{}^{III}$, line widths, Γ^{II} and Γ^{III}, and percent area, A^{II}, with $A^{III} = 100 - A^{II}$, are given in Table 1. Additional Mössbauer spectra of Prussian blue pigments are shown in Figure S4, and their parameters can be found in Table S2.

Prussian blue is a mixed valence ferric ferrocyanide complex, and the quadrupole doublet with an isomer shift of ca. −0.1 mm/s is assigned to low-spin iron(II) with a 6-fold carbon coordination environment, and the doublet with an isomer shift of ca. 0.4 mm/s is assigned to high-spin iron(III) with a 6-fold nitrogen coordination environment. The existence of inequivalent iron sites in Prussian blue has been also evidenced by X-ray photoelectron spectroscopy.[46,47] Detailed information about the assignment of the Mössbauer spectral components of Prussian blue pigments and several related iron cyanide complexes may be found in a recent paper.[48]

The Mössbauer spectral parameters given in Tables 1 and S2 and the line shape profiles shown in Figure 5 clearly reveal that the iron(III) quadrupole splitting shows a strong dependence upon the preparative method. The Prussian blues whose synthesis included a 2-h aging time of the Berlin white, **3**, and **S1**, **S4**, **S5**, **S6**, **S7**, and **S8**, have a less than 0.3 mm/s iron(III) quadrupole splitting. These small values are comparable to those observed for the commercial pigments **7** and **8**. Without further structural information, see below, it is not clear why the remaining **1**, **2**, and **4** pigments, as well as **S2**, **S3**, **S9**, **S10**, **S11**, **S12**, and **S13** have a relatively large iron(III) quadrupole splitting in comparison with the commercial pigments.

Another interesting spectral parameter is the iron(II) percent area, A^{II}, because the iron(III) to iron(II) ratio is expected to be 1 for the soluble and 4/3 for the insoluble Prussian blues; see Figure 6. Under the assumption of equal recoil-free fractions for

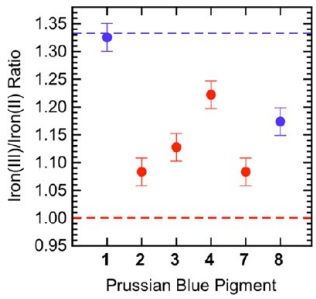

Figure 6. Iron(III) to iron(II) ratio for the insoluble, **1** and **8**, and soluble, **2**, **3**, **4**, and **7**, Prussian blue pigments. The observed ratios are rather different from the expected ratio of one for the soluble, red line, and 4/3 for the insoluble, blue line, pigments.

iron(II) and iron(III) ions, the experimental ratios are, however, often quite different from the expected ratios, indicating that the stoichiometries given in Table 1 are approximate.

It is well-known that the Mössbauer spectral parameters are temperature dependent. Therefore, because of its well-defined 295 K spectrum, the temperature dependence of the spectra of pigment **7** has been measured between 4.2 and 295 K. The resulting spectra obtained between 7 and 225 K are very similar to that of **7** obtained at 295 K and shown in Figure 5; the resulting spectral fitting parameters are given in Table S3, and the temperature dependence of both the iron(II) and iron(III) isomer shifts and the logarithm of the spectral absorption area is shown in Figure 7. The temperature dependence of the latter parameters has been fit with the Debye model[49] for a solid as is shown by the solid line in Figure 7.

A fit of the isomer shifts yields a Mössbauer temperature, Θ_M, of 670(50) K for the low-spin iron(II) ion and 490(10) K for the high-spin iron(III) ion in **7**. Further, a fit of the logarithm of the total spectral absorption area yields a Debye temperature, Θ_D, of 285(5) K for **7**. The observed Debye temperature is consistent with the near temperature independence of the iron(III) to iron(II) ratio observed for **7**. As expected,[49] the Θ_M and Θ_D temperatures obtained from the two temperature dependencies are different because they depend, for the isomer shift, on $\langle v^2 \rangle$, the mean-square vibrational velocity of the iron-57, and, for the absorption area, on $\langle x^2 \rangle$, the mean-square displacement of iron-57; unfortunately, there is no model independent relationship between these mean-square values.[49] However, measurements of the Mössbauer temperatures on various compounds[50] indicate that Θ_M is often twice as large as Θ_D; that is, the isomer shift is more sensitive to higher energy phonons.

At 4.2 K the Mössbauer spectrum of **7** clearly indicates that the pigment has undergone partial magnetic ordering. As a result, the spectra have been measured between 10 and 4.2 K with a velocity range of ±10 mm/s; see Figure 8. At 10 and 7 K there is no indication of any magnetic ordering, and the spectral parameters are the same as observed in the spectra obtained at ±3 mm/s. However, upon further cooling to 4.2 K, fits of the spectra clearly indicate that the high-spin iron(III) is ferromagnetically ordered

dx.doi.org/10.1021/jp3111327 | J. Phys. Chem. C 2013, 117, 9693−9712

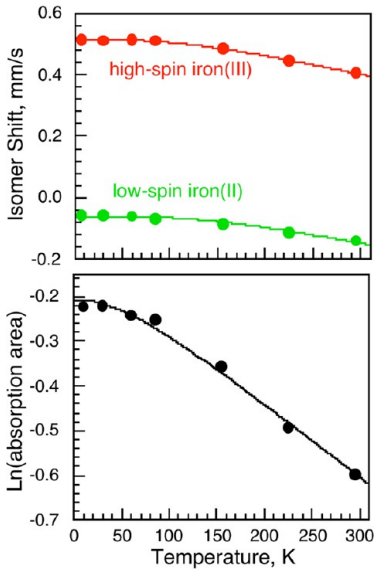

Figure 7. Temperature dependence of the isomer shift and logarithm of the spectral absorption area obtained for the commercial $KFe^{III}[Fe^{II}(CN)_6]\cdot xH_2O$, **7**, pigment. The solid lines represent fits with the Debye model for a solid. The errors are no larger than the size of the data points.

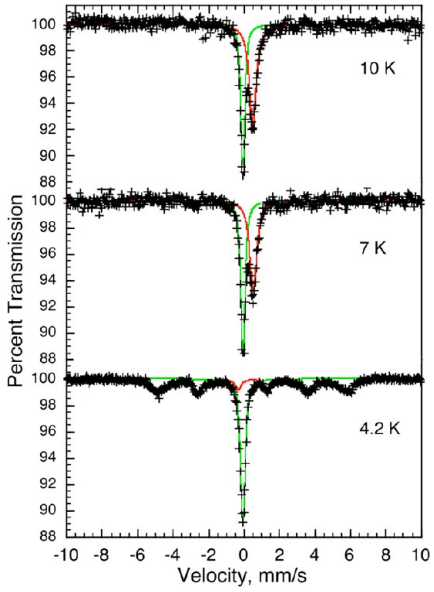

Figure 8. Mössbauer spectra of the commercial $KFe^{III}[Fe^{II}(CN)_6]\cdot xH_2O$, **7**, pigment obtained at the indicated temperatures. The green and red solid lines represent the low-spin iron(II) and high-spin iron(III) components, respectively.

with a hyperfine field of 33(1) T, whereas the low-spin iron(II) exhibits no magnetic order as is expected for a low-spin diamagnetic iron(II) ion with a t_{2g}^6 electronic configuration. An ordering temperature of 5.5(5) K has been reported[5] earlier for both soluble and insoluble Prussian blue. All of the remaining spectral parameters obtained at 4.2 K are consistent with their temperature dependence observed between 7 and 295 K; see Table S3. On the basis of the observed 4.2 K isomer shift of 0.49(1) mm/s and the quadrupole splitting 0.10(4) mm/s of the magnetic sextet, it is clear that this sextet must arise from the high-spin iron(III) in **7** even though the 33(1) T hyperfine field is similar to the 33.76(2) T field found for α-iron at 4.2 K. Further, α-iron at 4.2 K has an isomer shift of 0.114(4) mm/s and a quadrupole splitting of 0.000(2) mm/s, values that are not possible for the sextet observed in **7**. The hyperfine field of 33(1) T observed herein at 4.2 K compares well with the hyperfine field of 54(2) T observed[5] at 1.6 K if the temperature dependence of the hyperfine field is assumed to follow a Brillouin curve for $S = 5/2$. Indeed, at a reduced temperature of 4.2/5.5 = 0.764, the Brillouin curve predicts a hyperfine field that is 0.67 times the saturation field of 54 T, that is, 36 T.

As is evident from Figure 8, the magnetic sextet lines of the 4.2 K spectrum are asymmetrically broadened. In the fit, this broadening was accounted for by introducing a unitless incremental line width broadening, $\Delta\Gamma$, defined as $\Gamma(v) = \Gamma^{III} + (v - \delta^{III})\Delta\Gamma$, where v is the velocity, δ^{III} is the iron(III) isomer shift, and Γ^{III} is the line width at $v = \delta^{III}$. This broadening at 4.2 K may result from the proximity of the Curie temperature of 5.5 K, the presence of nonrandom vacancies as shown by the structural study, the deviation of **7** from the ideal stoichiometry of a soluble Prussian blue pigment, or a particle size distribution about the average size of ca. 70 nm; see above.

In the 4.2 K fit shown in Figure 8, the quadrupole splitting, ΔE_Q^{III}, and the angle, θ, between the principal axis of the electric field gradient tensor and the hyperfine field were alternatively refined. The quadrupole splitting was constrained to remain close to the paramagnetic ΔE_Q^{III} of +0.12 mm/s observed at 7 K. The best fit corresponded to a quadrupole splitting of +0.10(4) mm/s and a θ of 75(1)° or a ΔE_Q^{III} of −0.10(4) mm/s and a θ of 40(1)°. The parameter, $S_1 - S_2 = \Delta E_Q^{III}(3\cos^2\theta - 1)$ of +0.37(15) mm/s reported[5] by Ito et al., that is, the difference in the splittings between lines 1 and 2 and lines 5 and 6 of the iron(III) sextet, corresponds to a quadrupole splitting, ΔE_Q^{III}, varying between 0.185(75) and −0.37(15) mm/s for a θ varying from 0° to 90°, respectively. Hence, the absolute value of their quadrupole splitting, ΔE_Q^{III}, is larger than the quadrupole splitting observed in **7**. This large quadrupole splitting may be an indication of the presence of large strains in the sample studied[5] by Ito et al.; see below.

In conclusion, the Mössbauer spectra indicate that ferric ferrocyanide complexes have been synthesized. However, their observed iron(III) to iron(II) spectral area ratio does not always correspond to the expected value based on the ideal chemical formulas of insoluble and soluble Prussian blue pigments. Hence, quantitative chemical analyses must be obtained to understand these differences; see below. Further, large variations in the iron(III) quadrupole splitting are observed depending on the preparative method. Because the iron(III) quadrupole splitting depends upon the symmetry of the charge distribution at the iron(III) nucleus, both the crystal structure and the local ordering must be studied in detail by other methods.

Elemental Composition. The weight % iron and potassium content in the Prussian blue pigments **1**−**4**, **7**, and **8**, have been determined with an accuracy of ±0.01 wt % by atomic absorption and flame emission spectroscopy; see Figure 9. In this figure, the observed iron and potassium contents are compared to the expected contents, calculated from the stoichiometry of the insoluble $Fe_4[Fe(CN)_6]_3\cdot yH_2O$ and soluble $KFe[Fe(CN)_6]\cdot xH_2O$ and $NH_4Fe[Fe(CN)_6]\cdot xH_2O$ Prussian blue pigments. Because the exact degree of hydration is often unknown or difficult to determine, these calculations have assumed that the number of water molecules for the soluble pigments **2**, **3**, **4**, and **7** may range[51] from $x = 1$ to 5, whereas for the insoluble pigments **1** and **8** it may range[23] from $y = 14$ to 16, as usually reported in the literature. The corresponding ranges of

dx.doi.org/10.1021/jp3111327 | J. Phys. Chem. C 2013, 117, 9693−9712

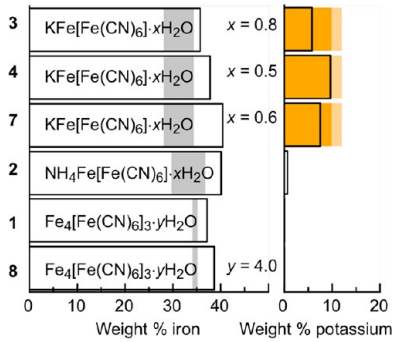

Figure 9. Observed weight % iron and potassium contents are given by the black rectangles, for **1**−**4**, **7**, and **8**. The range of iron content is shown in gray at left for x = 5 to 1 for **2**, **3**, **4**, and **7**, and for y = 16 to 14 for **1** and **8**. The potassium contents for these x-ranges are given in dark and light orange at right. The x and y values given in the center are obtained from thermogravimetric measurements.

weight % iron content for these degrees of hydration are shown in gray in the left portion of Figure 9.

Thermogravimetric analysis has been used to best estimate the weight % water content in selected pigments; the resulting curves are shown in Figures S5 and S6, and the resulting number of water molecules is given in the center of Figure 9. These values are unexpectedly small and most likely correspond to the amount of the zeolitic water molecules present in the pigment. The remaining coordinated water molecules are lost between 175 and ca. 250−260 °C, and this loss overlaps in part with the dramatic loss of the CN^- anions that begins at ca. 260 °C. Thus, both because the amount of coordinated water molecules could not be precisely determined and because the value of x may change with time and the history of a specific pigment, we have chosen to specify their water content as xH_2O throughout this article.

In general, the Prussian blue pigments have a slightly higher iron weight % content than is expected from the expected stoichiometry. In contrast, the potassium weight % content is lower than expected; see the right portion of Figure 9. The elemental analysis of pigment **7** reveals the presence of potassium cation, and thus **7** is a soluble Prussian blue. The compositions of insoluble Prussian blue pigments **1** and **8** are more complex because of the presence of nonrandom vacancies in the lattice. Theoretically, a quarter of the expected $[Fe^{II}(CN)_6]^{4-}$ anionic groups are missing, and their absence leads to an iron(III) to iron(II) ratio of 4/3, a value that is larger than that obtained from Mössbauer spectroscopy; see Figure 6.

To complete the elemental characterization of **1**−**4**, **7**, and **8**, the presence of impurities, if any, was determined by particle-induced X-ray emission studies; see the Supporting Information for experimental details and specific results given in Table S4. In general, the iron and potassium content observed for **1**−**4**, **7**, and **8** is in good agreement with the above analysis. Finally, the composition and molecular formula of selected Prussian blue pigments calculated from the results obtained by elemental and thermogravimetric analysis and Mössbauer spectroscopy are graphically presented in Figure S7.

On the basis of the Mössbauer spectral results, the thermogravimetric analyses, the atomic absorption and flame emission spectral results, and the particle X-ray emission studies, one can conclude that (i) the apparent solubility of Prussian blue only relies on the presence of alkali cations, (ii) from the Fe(II) to Fe(III) ratio it is impossible to distinguish the soluble from the insoluble variety, and (iii) the typically reported stoichiometries of $KFe^{III}[Fe^{II}(CN)_6]\cdot xH_2O$ and of $Fe_4^{III}[Fe^{II}(CN)_6]\cdot xH_2O$ are only approximately correct because of the presence of vacancies and a variable amount of water molecules in both the soluble and the insoluble varieties. The structure and the stoichiometry of the soluble and insoluble Prussian blues will be revisited on the basis of Rietveld refinement of high-resolution X-ray diffraction data and of pair distribution analysis.

Prussian Blue Crystal Structures. To investigate their crystal structures, the Prussian blue pigments **1**−**4**, **7**, and **8** have been studied by powder X-ray diffraction; the resulting patterns are shown in Figure 10 along with expanded patterns for **7** and **8** that better reveal the weak reflections in these two very well-crystallized pigments.

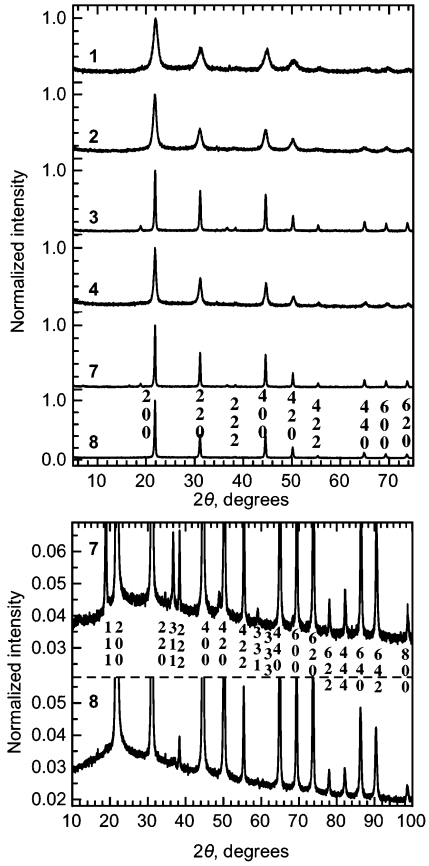

Figure 10. X-ray powder diffraction patterns of Prussian blue pigments **1**−**4**, **7**, and **8**. The intensity of the diffraction has been normalized to that of the most intense (200) reflection. The patterns of pigments **7** and **8** recorded over 2θ ranging from 10° to 100°, with a time per step of 15 s, have been expanded to better show the weak reflections.

Prussian blue pigments are reported to crystallize in the $Fm3m$ space group, and their X-ray diffraction reflections can be mostly indexed accordingly. In a face-centered cubic structure, the hkl indices must be either all even or all odd. The pigment **7** exhibits some additional weak face-centered reflections. Moreover, the reflection intensities observed for **7** and **8** also differ, indicating the expected somewhat different crystal structures. In addition to the differences in the intensities of the reflections, the patterns of the various Prussian blue pigments also show large differences in reflection broadening; see Figure 10. The unaged pigments **1**, **2**, and **4** exhibit broader peaks than **3** whose preparative method included an aging of Berlin white for 2 h; pigment **3** also exhibits reflections as broad as those of the commercial pigments **7** and **8**.

dx.doi.org/10.1021/jp3111327 | J. Phys. Chem. C 2013, 117, 9693−9712

Table 2. Particle Size and Strain in the (*h*00) Crystallographic Direction

	particle size, nm				strain, %
	Scherrer		Williamson−Hall		
expected composition	*h*00	*hh*0	*h*00	*hh*0	*h*00
$Fe_4^{III}[Fe^{II}(CN)_6]_3{\cdot}xH_2O$ (**1**)	7(1)	6(1)	6(1)	6(1)	1.2(3)
$NH_4Fe^{III}[Fe^{II}(CN)_6]{\cdot}xH_2O$ (**2**)	9(1)	8(1)	11(1)	10(1)	0.6(4)
$KFe^{III}[Fe^{II}(CN)_6]{\cdot}xH_2O$ (**3**)	39(1)	34(1)	43(1)	44(1)	0.11(3)
$KFe^{III}[Fe^{II}(CN)_6]{\cdot}xH_2O$ (**4**)	14(1)	12(1)	27(1)	18(1)	1.4(5)
$KFe^{III}[Fe^{II}(CN)_6]{\cdot}xH_2O$ (**S1**)	16(1)	13(1)	22(1)	21(1)	0.8(6)
$KFe^{III}[Fe^{II}(CN)_6]{\cdot}xH_2O$ (**S2**)	13(1)	11(1)	22(1)	15(1)	1.6(7)
$KFe^{III}[Fe^{II}(CN)_6]{\cdot}xH_2O$ (**7**)	54(1)	43(1)	96(1)	84(1)	0.45(1)
$Fe_4^{III}[Fe^{II}(CN)_6]_3{\cdot}xH_2O$ (**8**)	44(1)	38(1)	65(1)	81(1)	0.40(9)

By applying the Scherrer[52] and Williamson−Hall methods[53] to the diffraction reflection broadening, it is possible to obtain the average crystallite size and strain present in the Prussian blue pigments; see the Supporting Information for details about the application of these methods and the procedure used to deconvolute the pure reflection profile from the experimentally observed profile.

Size Effect and Strain. A Williamson−Hall[53] plot yields information about the particle size in a sample to the extent that the width of the X-ray diffraction reflections is larger than the instrumental contribution. For pigments that exhibit X-ray reflection broadening, their particle size in a specific crystallographic direction can be determined with either the Williamson−Hall[53] or the Scherrer[52] method; see Table 2. The relatively small number of reflections in the Williamson−Hall plots, see Figure S8, leads to the relatively large error given in Table 2.

Not surprisingly, the Scherrer method yields smaller values for particle size because the reflection broadening due to any strain present is not considered. The method of pigment preparation leads to the smallest particles for **1**. Two hours of aging in an ambient atmosphere does not significantly increase the particle size, as is shown for **S1** in Table 2, a pigment that does not contain larger particles than **4** or **S2**. In contrast, the aged pigments **3**, **7**, and **8** have larger particle sizes and excellent color properties for a blue pigment. All of these latter pigments were prepared according to patented methods that take place under a nitrogen atmosphere and include an aging step of the Berlin white precipitate prior to its oxidation to form Prussian blue. The particle sizes of **3**, **7**, and **8** were determined by scanning electron microscopy to be between 60 and 80 nm; see Figure 4. However, it is difficult to know whether the particle size measured in the scanning electron micrographs corresponds to the crystallite size, that is, the coherence length obtained from the microstructural diffraction analysis.

For some Prussian blue pigments, such as **4**, **7**, and **8**, the particle size in the (*hh*0) crystallographic direction differs slightly from that determined from the (*h*00) reflections, indicating a small anisotropy in their crystal morphology.

The Williamson−Hall method[53] yields an estimate of the strain due to the presence of lattice defects in the crystallites. Whereas the reflection broadening due to crystallite size effects depends on the Bragg angle as $1/\cos\theta$ following the Scherrer formula, the reflection broadening due to strain varies as $\tan\theta$. The larger is the slope of the correlation of the reflection broadening versus $2\sin\theta/\lambda$, where the reflection broadening is expressed as $\beta\cos\theta/\lambda$ and β is the reflection broadening less any instrumental broadening in this case of the (*h*00) reflections, the larger is the strain. All of the Prussian blues exhibit strain, see Table 2, a strain that shows a weak correlation with the iron(III) quadrupole splitting observed by iron-57 Mössbauer spectroscopy; see Table 1 and Figure 11. A larger percent strain is accompanied by a larger iron(III) quadrupole splitting, the latter of which is a measure of the asymmetry in the iron(III) electronic environment. A weak linear correlation, see Figure 11, is observed for all of the Prussian blue pigments except for **4** and **S2**, pigments that exhibit a rather large strain for a relatively small iron(III) quadrupole splitting. The large value of the percent strain observed for **4** and **S2** may result from the inaccuracy in determining the integral width of the (600) reflection because of its weak intensity. However, a large strain is not unexpected for pigments **4** and **S2**, which were not aged during their synthesis. Indeed, this large strain decreases when an aging step is introduced in the synthesis of pigments **3** and **S1**.

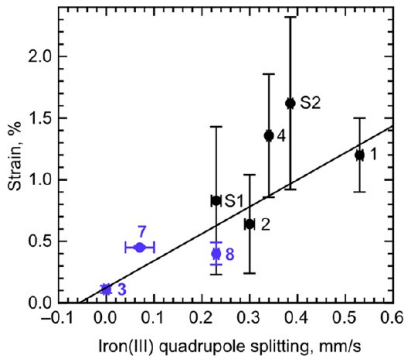

Figure 11. Percent strain versus the iron(III) quadrupole splitting, ΔE_Q^{III}, of the Prussian blue pigments. The blue points indicate the pigments with the best color qualities. Some of the errors do not show because they are the same as or smaller than the size of the data points.

Prussian Blue Crystal Structure Refinements. The presence of vacancies in Prussian blue is well-known. However, little research has been carried out to determine the distribution of these vacancies and its influence on the local structure and the properties of Prussian blue pigments. To overcome the lack of knowledge about the local structural arrangement and its influence on the intervalence electron transfer pathway, the Prussian blue samples have been studied by pair distribution analysis and iron K-edge X-ray absorption spectroscopy. The fit and interpretation of the results, see below, obtained by both techniques are based on the known structure[23] of insoluble Prussian blue. Although the crystal structure of insoluble Prussian blue is well-known, that of the soluble Prussian blues is still rather poorly understood. Thus, we have undertaken a Rietveld refinement of the X-ray powder diffraction patterns obtained for pigments **7** and **8**.

dx.doi.org/10.1021/jp3111327 | J. Phys. Chem. C 2013, 117, 9693−9712

A refinement of an X-ray powder diffraction pattern by the Rietveld method[54] typically requires a prior knowledge of the composition and a structural model for the sample understudy. The above compositional results have revealed that the Prussian blues under study are hydrated ferric ferrocyanide complexes, with a low impurity content; X-ray powder diffraction patterns also confirm the presence of a single crystalline phase. In a Rietveld refinement, the choice of the structural model is crucial, especially because the crystal structures of Prussian blue pigments are notoriously complex because of both their colloidal character and the possible presence of lattice vacancies. The average structure of an insoluble Prussian blue is generally described with the *Fm*3*m* space group, where a quarter of the $[Fe^{II}(CN)_6]^{4-}$ sites are vacant and replaced by water molecules; see Figure S9.[55] The water molecules in Prussian blue pigments can be either in the lattice vacancy and coordinated to iron(III), or hydrogen bonded to one of these coordinated water molecules, or completely interstitial in a zeolitic-like position. Accordingly, the stoichiometry is $Fe^{III}_4[Fe^{II}(CN)_6]_3{\cdot}xH_2O$, where x is between 14 and 16, that is, with 6 coordinated water molecules and 8−10 hydrogen-bonded or zeolitic-like water molecules.

The *Fm*3*m* space group implies a statistically random distribution of the vacancies in the lattice. However, in practice, in single crystals the $[Fe^{II}(CN)_6]^{4-}$ vacancies are often not randomly distributed, and the X-ray diffraction pattern indicates that the structure belongs to the lower symmetry *Pm*3*m* space group.[23] In the cubic primitive model, Buser et al.[23] introduced an occupancy parameter, p, that is the probability that the $[Fe^{II}(CN)_6]^{4-}$ site in the center of the unit cell is occupied; see Table 3. When p is zero the structure is completely ordered, and all occupancies are integral. A p value of 3/4 indicates that 1/4 of the $[Fe^{II}(CN)_6]^{4-}$ sites are vacant, the situation that corresponds to the cubic face-centered *Fm*3*m* model previously described.[23]

Table 3. Site Distribution and Occupancies in *Fm*3*m* and *Pm*3*m*

	*Fm*3*m*		*Pm*3*m*	
	Wyckoff position	occupancy	Wyckoff position	occupancy
4 Fe^{III}	4*a*	1	1*a*	1
			3*c*	1
3 Fe^{II}	4*b*	3/4	1*b*	p
			3*d*	$1 - p/3$
18 C	24*e*	3/4	6*e*	$1 - p/3$
			6*f*	p
			12*h*	$1 - p/3$
18 N	24*e*	3/4	6*e*	$1 - p/3$
			6*f*	p
			12*h*	$1 - p/3$
6 O	24*e*	1/4	6*e*	$p/3$
			6*f*	$1 - p$
			12*h*	$p/3$
8 O	8*c*	1	8*g*	1

The structure of an insoluble Prussian blue pigment is now well established, and the model developed[23,55] by Buser and Herren has been used as the initial model for the Rietveld refinement of the structure of **8**, a commercial insoluble Prussian blue pigment. By using the *Pm*3*m* space group and an occupancy parameter p, any possible nonrandom distribution of vacancies is taken into account.

Regarding the structure of soluble Prussian blue, the model developed[15] by Keggin and Miles in 1936 is usually taken as viable. It consists of a perfect cubic Fe^{II}−CN−Fe^{III} framework with no vacancies. The alkali cations and the water molecules are localized in the center of the lattice cavities, at zeolitic-like positions. Recently, this model for soluble potassium cation containing Prussian blue has been revisited[16] by Bueno et al. who studied electrochemically synthesized potassium cation containing ferric ferrocyanide by X-ray synchrotron radiation powder diffraction. They concluded that about 25% of the $[Fe^{II}(CN)_6]^{4-}$ sites were vacant. Moreover, they unexpectedly claimed that the potassium cations were part of the water crystalline substructure and occupied the 24*e* site in the *Fm*3*m* space group, with an x positional parameter only slightly different from that of the coordinated water. They proposed a new stoichiometry to describe the structure, $Fe^{3+}_4[Fe^{2+}(CN)_6]_3{\cdot}[K^+_h{\cdot}OH^-_h{\cdot}mH_2O]$. The charge balance is ensured by the presence of the appropriate number of OH^- anions, which compensate the positive charge of the potassium cations.

Rietveld refinements have been performed for the commercial soluble **7**, and insoluble **8**, Prussian blue pigments; see Tables 4 and 5 and Figure 12. Because the diffraction data previously shown in Figure 10 were inadequate for Rietveld analysis, high-energy X-ray powder diffraction patterns of **7** and **8** were recorded. The primitive cubic model reported[23] by Buser et al. with an occupancy parameter, p, was used as an initial structural model for both the soluble and the insoluble samples. The background was linearly interpolated. An isotropic Thomson−Cox−Hastings function was used to describe the reflection profiles. The instrumental profile was obtained from a LaB_6 pattern recorded in the same conditions. Refinement of the additional sample broadening parameters yielded values of particle size and strain very close to those reported above from Scherrer and Williamson−Hall methods. To reduce correlations between structural parameters, an overall isotropic atomic displacement parameter, common to all atoms, was refined. Individual isotropic atomic displacement parameters were constrained to zero for the iron cations and cyanide anions, to the same refined value for all of the water oxygens on the 6*e*, 6*f*, and 12*h* sites, and to an independent value for the water oxygens on the 8*g* site. The total atomic displacement parameters

Table 4. Lattice Parameter and Average Bond Distances

distance, Å	$Fe^{III}_4[Fe^{II}(CN)_6]_3{\cdot}xH_2O$ (**8**)	$Fe^{III}_4[Fe^{II}(CN)_6]_3{\cdot}15H_2O$[a]	$Fe^{III}_4[Fe^{II}(CN)_6]_3{\cdot}15H_2O$[b]	$KFe^{III}[Fe^{II}(CN)_6]{\cdot}xH_2O$ (**7**)	$Fe^{III}_4[Fe^{II}(CN)_6]_3{\cdot}[K_h{\cdot}OH_h{\cdot}mH_2O]$[c]
a	10.2178(1)	10.166(3)	10.155(4)	10.2059(1)	10.2058(1)
Fe(II)−C	1.830(4)	1.923(8)	1.92(1)	1.947(5)	1.86(6)
Fe(III)−N	2.096(2)	2.029(6)	2.01(1)	1.926(4)	2.00(7)
C−N	1.183(4)	1.131(6)	1.148	1.155(5)	1.17(4)
Fe(III)−O	2.297(10)	2.138(19)	1.96	2.568(15)	2.00(7)

[a]Lattice parameter and average bond distances as reported in ref 23. [b]Lattice parameter and average bond distances as reported in ref 55. [c]Lattice parameter and average bond distances as reported in ref 16.

dx.doi.org/10.1021/jp3111327 | J. Phys. Chem. C 2013, 117, 9693−9712

Table 5. Crystal Structure of Two Prussian Blue Pigments in the *Pm*3*m* Space Group[a]

		insoluble pigment, **8**, $p = 0.61(1)$			soluble pigment, **7**, $p = 0.72(1)$		
		$Fe^{III}_4Fe^{II}_{3.00(2)}(CN)_{18.0(1)}\cdot 11.2(1)H_2O$			$K_{1.9(2)}[Fe^{III}_4Fe^{II}_{3.00(2)}(CN)_{18.0(1)}]\cdot\{7.0(2)H_2O+1.9(2)OH\}$		
site		*x*	occupancy	*U*, Å^2	*x*	occupancy	*U*, Å^2
Fe(III)	1*a*	0	1	0.0096(1)	0	1	0.0113(1)
	3*c*	0	1	0.0096(1)	0	1	0.0113(1)
Fe(II)	1*b*	1/2	0.609(11)	0.0096(1)	1/2	0.736(11)	0.0113(1)
	3*d*	1/2	0.799(4)	0.0096(1)	1/2	0.755(4)	0.0113(1)
C	6*e*	0.3207(3)	0.7989(18)	0.0096(1)	0.2945(4)	0.7551(19)	0.0113(1)
	6*f*	0.3207(3)	0.6046(18)	0.0096(1)	0.2945(4)	0.7354(19)	0.0113(1)
	12*h*	0.1788(3)	0.7989(9)	0.0096(1)	0.1834(4)	0.7551(9)	0.0113(1)
N	6*e*	0.2074(2)	0.7989(18)	0.0096(1)	0.1887(3)	0.7551(19)	0.0113(1)
	6*f*	0.2074(2)	0.6046(18)	0.0096(1)	0.1887(3)	0.7353(19)	0.0113(1)
	12*h*	0.2971(2)	0.7989(9)	0.0096(1)	0.3113(3)	0.7551(9)	0.0113(1)
O	6*e*	0.2248(7)	0.2021(18)	0.225(8)	0.2478(11)	0.2451(19)	0.191(6)
	6*f*	0.2248(7)	0.3964(18)	0.225(8)	0.2478(11)	0.2649(19)	0.191(6)
	12*h*	0.2752(7)	0.2021(9)	0.225(8)	0.2714(11)	0.2450(9)	0.191(6)
	8*g*	0.2469(16)	0.649(5)	0.110(3)	0.23051	0.356(16)	0.035(3)
K	8*g*				0.23051	0.107(13)	0.070(8)
	8*g*				0.28715	0.129(10)	0.070(8)

[a]The values given in parentheses are the estimated standard deviations. Their absence indicates that the parameter was constrained to the value given.

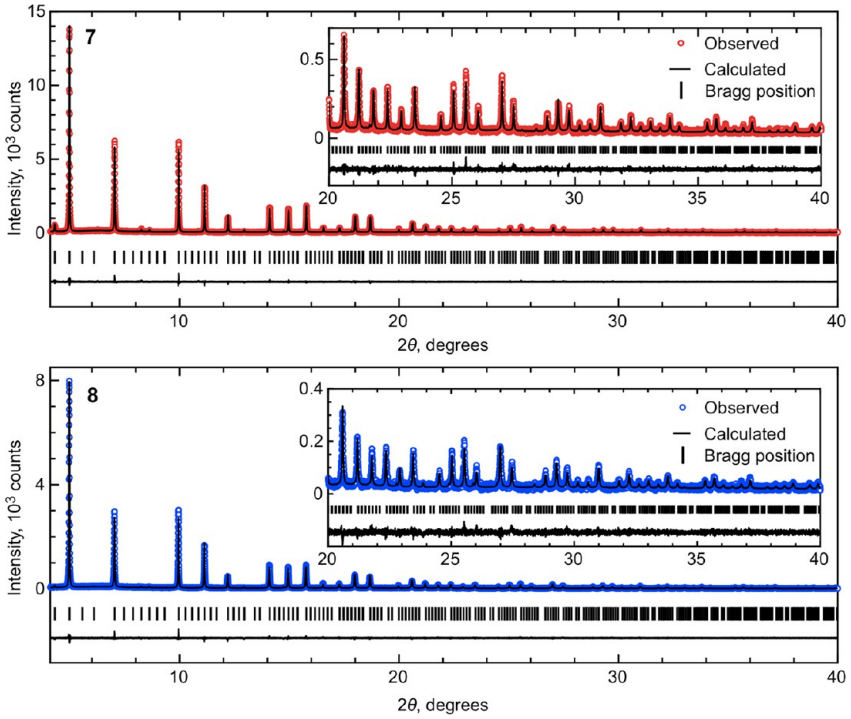

Figure 12. Rietveld refinement of the high-resolution X-ray powder diffraction patterns of $KFe^{III}[Fe^{II}(CN)_6]\cdot xH_2O$, **7**, with $R_p = 15.3\%$, $R_{wp} = 15.5\%$, $\chi^2 = 1.031$, and $R_{Bragg} = 3.87\%$ (top) and $Fe^{III}_4[Fe^{II}(CN)_6]_3\cdot xH_2O$, **8**, with $R_p = 18.3\%$, $R_{wp} = 19.6\%$, $\chi^2 = 0.962$, and $R_{Bragg} = 5.03\%$ (bottom).

reported in Table 5 on a given site are obtained by summing the overall and corresponding individual atomic displacement parameters. Moreover, soft constraints were used to limit the Fe−O bond distances within the range reported in the literature.

The Rietveld refinement for **8**, see the lower portion of Figure 12, yields an occupancy parameter, *p*, of 0.61(1) for the iron(II) 1*b* site, indicating that the central $[Fe^{II}(CN)_6]^{4-}$ site is vacant with a 39% probability. The occupancy parameter is thus lower than expected in the *Fm*3*m* model, which is characterized by an occupancy parameter of 3/4 = 0.75 that indicates a random distribution of vacancies. Thus, sample **8** presents a rather high degree of ordering of the $[Fe^{II}(CN)_6]^{4-}$ vacancies.

The resulting lattice parameter and the bond distances obtained for **8** are compared to those previously published[16,23,55] in Table 4. More specifically, the lattice parameter of $a = 10.2178(1)$ Å obtained for **8** is significantly larger than the values of $a = 10.166(3)$ and $10.155(4)$ Å reported[23,55] earlier. The atomic displacement parameter values of the oxygens are unusually large, but various attempts to constrain them to standard values led to significantly worse refinements. Such large values may result from displacement disorder of the oxygens

dx.doi.org/10.1021/jp3111327 | J. Phys. Chem. C 2013, 117, 9693−9712

because of their different natures, such as in the OH^- anion and in a water molecule, and their different environments, such as in coordination with an iron(III) ion or in a zeolitic-like position. This displacement disorder could also explain why some refined bond distances such as Fe(III)−O are different from those given in the literature.

For pigment **8**, the Rietveld refinement yields 11.2(1) oxygens, of which six on the 6*e*, 6*f*, and 12*h* sites in the *Pm*3*m* space group correspond to water bonded to the open iron(III) coordination sites adjacent to the missing $[Fe^{II}(CN)_6]^{4-}$ anion. The remaining 5.2(1) uncoordinated water molecules are on the 8*g* site in the *Pm*3*m* space group, and either occupy zeolitic-like positions or are hydrogen bonded to the coordinated water. This 5.2(1) water content of 8.8 wt % is in relatively good agreement with the 7.7 wt % loss of four uncoordinated water molecules between room temperature and ca. 175 °C for **8** as determined by thermogravimetric analyses.

The Rietveld refinement of soluble potassium cation containing Prussian blue pigment **7** yields interesting results. First, our attempts to use the model proposed by Bueno et al.[16] for the Rietveld refinement failed in reproducing correctly the intensities of several weak reflections. In contrast, it appears that the cubic primitive *Pm*3*m* space group used above for refining the insoluble Prussian blue, **8**, is perfectly suitable for the soluble variety. The occupancy parameter, *p*, refines to a value of 0.72(1), which is close to the 0.75 value expected for the *Fm*3*m* space group. Therefore, the vacancies are almost randomly distributed in **7**. Furthermore, the successful refinement in the *Pm*3*m* space group indicates that the previously proposed[16] structural model for the soluble $KFe^{III}[Fe^{II}(CN)_6]\cdot xH_2O$ Prussian blue, where the lattice does not contain any vacancies, must be revised.

To locate the potassium cations, Fourier difference maps obtained on the structure of **7** without the potassium cations were computed; see Figure 13. Potassium cations occupy the 8*g*

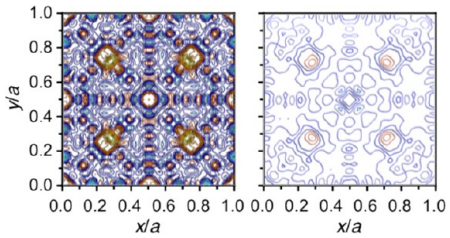

Figure 13. Fourier difference maps obtained for **7** with a = 10.2059(1) Å, the potassium cations removed, and all of the layers between z/a = 0 and 1 superimposed with a z/a increment of 0.02 (left) and at the z/a = 0.28 layer alone (right). An excess of electron density, in red, appears in the zeolitic-like positions, attributed to the presence of the potassium cations.

site at the center of the cell octants as is evidenced by an excess of electron density appearing in red at the center of the cell octants, that is , in the zeolitic-like positions. This potassium cation location disagrees with the structure proposed[16] by Bueno et al., in which the potassium cations are part of the crystalline substructure, but agrees with the first structure described[15] by Keggin and Miles. At this point, it is relevant to point out that the high-resolution powder diffraction pattern of **7** shown in Figure 12 exhibits far higher resolution and lower incoherent scattering that the pattern used[16] by Bueno et al., in their analysis and shown in Figure 1 of their paper. The pattern shown in Figure 12 exhibits ca. 50 reflections, whereas the pattern published[16] by Bueno et al. exhibits 13−15 reflections. The large difference in the quality of the data, as well as a different preparation of the soluble Prussian blue sample, may account for many of the differences reported[16] by Bueno et al., as compared to the result found herein for **7**; see Table 4.

The potassium cations and the oxygens in the zeolitic-like positions were first assumed to occupy two distinguishable 8*g* sites. Such a refinement yields 0.83(7) potassium cations and 4.78(1) water molecules. This potassium content, which corresponds to 3.0 wt %, is smaller than the expected potassium content of 7.5 wt %, that is, ca. two cations per unit cell, as determined by flame emission spectroscopy. Furthermore, the uncoordinated water content is larger than the value of 4.4 wt % determined by the thermogravimetric analysis of **7**; see Figures S5,S6. To better match the elemental composition previously determined for **7**, a different refinement approach was used. Because the previous refinement led to a deficit in potassium cations and an excess of oxygens, the potassium cations were assumed to also occupy the 8*g* oxygen position. In other words, oxygens and potassium cations may share the same zeolitic-like position. This assumption is valid because X-ray diffraction does not distinguish different species occupying the same site. The number of potassium cations per unit cell was then constrained to the value obtained by flame emission spectroscopy, that is, 1.9 cations per unit cell. This revised refinement yields 2.86(16) zeolitic water molecules, corresponding to 4.7 wt %, in good agreement with the 4.4 wt % determined by thermogravimetric analysis. Consequently, the Prussian blue pigment **7** contains 6.0(1) coordinated oxygens and 2.9(2) uncoordinated oxygens, that is, a total of 8.9(2) oxygens. To balance the charge of the 1.9(2) potassium cations, 1.9(2) of these oxygens must be part of OH^- anions. The exact location of the OH^- anions could not be precisely determined by X-ray diffraction. The stoichiometry of **7** can thus be described by the formula $K_{1.9(2)}[Fe^{III}_4Fe^{II}_{3.00(2)}(CN)_{18.0(1)}]\cdot\{7.0(2)H_2O+1.9(2)OH\}$.

In conclusion, the Keggin and Miles model[15] for soluble potassium cation containing Prussian blue has been revised by using high-resolution X-ray diffraction patterns obtained with synchrotron radiation of short wavelength. The structure of soluble Prussian blue pigments appears to be very similar to that of insoluble Prussian blue because it also contains ca. 25% of $[Fe^{II}(CN)_6]^{4-}$ vacancies.

Pair Distribution Analysis of the Pigment Short-Range Order. To study the local structural configuration of the Prussian blue pigments, very high-energy X-ray powder diffraction and iron K-edge X-ray absorption spectroscopy experiments were carried out on the ID11 and BM26 beamlines at the ESRF, Grenoble, France.

Whereas coherent Bragg scattering of X-rays provides the average long-range structural information, the diffuse X-ray scattering corresponds to two-body correlations that are related to any structural short-range disorder and local distortions in a compound.[28] The broadening of the reflections in this function depends on the distance distribution around the average value that results from thermal vibrations or positional disorder. The pair distribution functions for pigments **7** and **8** are compared in the upper panel in Figure 14. Both functions have been obtained with a Gaussian damping of 20 $Å^{-1}$ and a Q_{max} of 30 $Å^{-1}$. It is immediately obvious that the two functions are very similar, with an additional broadening of the peaks in the pair distribution function obtained for pigment **7**. Hence, pigments **7** and **8** have very similar short-range order. Further, the insoluble pigment **8** exhibits slightly narrower peaks in its distribution than does **7**, an indication of a higher degree of ordering in **8** than **7**. This

dx.doi.org/10.1021/jp3111327 | J. Phys. Chem. C 2013, 117, 9693−9712

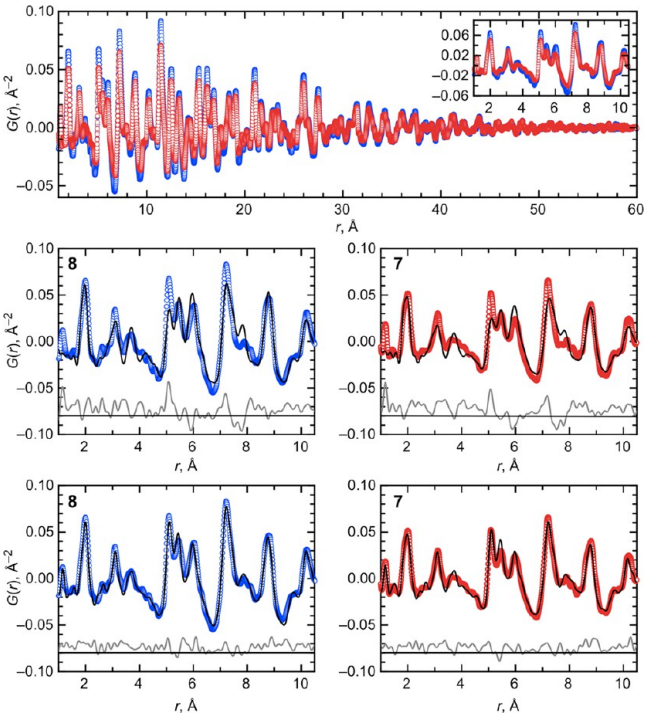

Figure 14. Pair distribution functions of pigments **7**, red ○, and **8**, blue ○, obtained with a Gaussian damping of 20 $Å^{-1}$ and a Q_{max} of 30 $Å^{-1}$, top panel. Refinement of the pair distribution function, $G(r)$, for pigments **8**, left, and **7**, right, obtained with the average *Pm*3*m* structure and occupancy, *p*, of 0.61 and 0.72, respectively, center panels, and with a random distribution of three different substructures containing zero, one, and two vacancies, bottom panels.

narrower distribution is consistent with the occupancy, p = 0.61(1) obtained for **8**, determined by Rietveld refinement as compared to the p = 0.72(1) obtained for **7**.

Finally, the pair distribution functions of both pigments were fitted with the PDFGui software.[30] The results of the pair distribution analysis of soluble pigment **7** and insoluble pigment **8** are shown in Figure 14, middle and lower panels. The quality of a pair distribution refinement is given by two agreement factors similar to those used for a Rietveld refinement, R_w, and a reduced χ^2, which is equivalent to the χ^2 factor divided by the number of degrees of freedom.

The effect of the experimental resolution on the pair distribution function was determined by fitting the pair distribution of a LaB_6 standard recorded in the same conditions. This effect manifests itself by the decrease of peak amplitudes at longer distances, as seen in the top panel of Figure 14. The pair distribution was first fitted for **7** and **8**, respectively, and then the same model has been applied to pigments **3** and **4**.

As evidenced by the Rietveld refinement, insoluble pigment **8** crystallizes in the *Pm*3*m* space group with an occupancy parameter p of 0.61(1) for the 1*b* site, indicating a probability of 39% of having the central $[Fe^{II}(CN)_6]^{4-}$ site vacant. This model is believed to be suitable to describe the long-range ordering. In contrast, it fails to describe the local order on a length-scale shorter than or comparable to the lattice parameter; see the middle portion of Figure 14. The difficulty in refining the crystal structure of Prussian blue pigments results from the inherent structural disorder arising from the presence of vacancies, a disorder that is characteristic of all cubic polynuclear transition metal-cyanides complexes.[12] As Herren et al.[55] proposed, the structure of an insoluble Prussian blue pigment, that is, $Fe_4^{III}[Fe^{II}(CN)_6]_3 \cdot xH_2O$, **8**, can be considered as a sum of ordered substructures containing zero to four $[Fe^{II}(CN)_6]^{4-}$ vacancies, vacancies whose relative probabilities are given by a binomial distribution if the substructures are randomly distributed.

If the occupancy parameter, p, is 0.75, in the *Pm*3*m* space group, as was proposed by Herren et al.[53] in the *Fm*3*m* space group, the probability of having in a given unit cell 0, 1, 2, 3, or 4 vacant $[Fe^{II}(CN)_6]^{4-}$ sites, whose iron(II) ion positions are the 1*b* and/or 3*d* crystallographic sites, is 31.6%, 42.2%, 21.1%, 4.7%, and 4%, respectively. In the above Rietveld refinements, the refined occupancy parameter, p, yields the probability of having the central iron(II) ion only on the 1*b* site. Hence, a p value of 0.61 indicates that additional $[Fe^{II}(CN)_6]^{4-}$ vacancies occur on the 3*d* positions with a $p/3$ of ca. 0.2 probability. In the bond-length range of one unit cell, the pair distribution function of Prussian blue can be considered as the sum of the pair distribution functions of unit cells containing 0, 1, 2, 3, or 4 ordered vacancies, weighed by their respective probabilities.

The pair distribution function for **8** was thus refined by building a three "phase" model, with "phases" labeled A, B, and C, corresponding to "substructures" in which there are zero, one, and two $[Fe^{II}(CN)_6]^{4-}$ vacancies, respectively. The substructures with three and four vacancies were neglected for simplicity, because of their small probability. The corresponding phases are shown in Figure S10. Cell parameters and linear atomic correlation factors were considered equal for the three structures, and their scale factors were refined. Constraints resulting from the space group symmetry *Pm*3*m* were applied to the atomic positional parameters. Individual isotropic atomic displacements parameters were refined for the iron ions and were constrained to be the same in the Fe(II)−C and Fe(III)−N octahedra. Isotropic atomic displacement parameters were constrained to the same refined value for all of the water oxygens on the 6*e*, 6*f*, and 12*h* sites, and to an independent value for the water oxygens on the 8*g* site. Hydrogen atoms were not introduced. Because the refinement range was limited to one unit cell, all occupancy parameters were fixed to unity. This led to a total of 34 independent refined parameters.

The relative phase content can be determined by considering both the scale factor and the atomic content of the unit cell. It should be noted that each contribution in the pair distribution function is weighed according to the product of the scattering

Table 6. Lattice Parameters and Bond Distances Obtained from the Pair Distribution Analysis

pigment	lattice parameter, *a*, Å	Fe(II)−C distance,[a] Å	Fe(III)−N distance,[a] Å	C−N distance,[a] Å	Fe(III)−O distance,[a] Å
$KFe^{III}[Fe^{II}(CN)_6]\cdot xH_2O$ (**3**)	10.17(1)	1.93(8)	2.01(6)	1.17(8)	2.3(2)
$KFe^{III}[Fe^{II}(CN)_6]\cdot xH_2O$ (**4**)	10.16(1)	1.95(9)	1.94(8)	1.18(7)	2.2(1)
$KFe^{III}[Fe^{II}(CN)_6]\cdot xH_2O$ (**7**)	10.18(1)	1.96(9)	1.99(6)	1.18(6)	2.3(2)
$Fe_4^{III}[Fe^{II}(CN)_6]_3\cdot xH_2O$ (**8**)	10.17(1)	1.92(5)	2.04(4)	1.13(6)	2.5(1)

[a]The values in parentheses correspond to the standard deviation of a given interatomic distance taken over the three substructures.

dx.doi.org/10.1021/jp3111327 | J. Phys. Chem. C 2013, 117, 9693−9712

factor of the atoms; see the Supporting Information for details. This model leads to a much better refinement of the pair distribution in **8** as may be seen in the lower left portion of Figure 14; the center left fit with a random distribution of the $[Fe^{II}(CN)_6]^{4-}$ vacancies and $p = 0.61$ yields $R_{wp} = 33.3\%$ and $\chi^2 = 0.581$, whereas the bottom left fit with the three phases yields $R_{wp} = 17.1\%$ and $\chi^2 = 0.153$.

Although the refined lattice parameter and bond distances obtained for the three-phase model are consistent within statistical error with those obtained from the Rietveld refinement of the X-ray diffraction of **8**, see Table 6, the agreement between the observed and calculated pair distribution is not as perfect as desirable. This disagreement may result from the neglect of the phases with three and four vacancies. Furthermore, different local atomic distortions are expected to occur in the three phases, because of their different vacancy distributions, distortions that could not be taken into account in the refinements. The model corresponds to a relative phase content in term of one unit cell of 13(2)%, 39(2)%, and 48(2)% for phases A, B, and C, respectively. These values are different from those calculated above from the binomial distribution, indicating that the probability of having an iron(II) ion in positions 1*b* is lower than the average probability of 0.75, in agreement with the occupancy parameter, *p*, of 0.61 determined by Rietveld refinement.

A similar fitting procedure was applied to refine the pair distribution function observed for the soluble Prussian blue pigment **7**. The resulting refinements are shown at the right in Figure 14.

The agreement between the calculated and observed pair distribution analysis is far better with the model including the three phases, A, B, and C, than the average *Pm*3*m* model with an occupancy parameter of 0.72. In this case, the refinement, center right, with $p = 0.72$ yielded $R_{wp} = 41.6\%$ and $\chi^2 = 0.351$, whereas the refinement with three different phases, A, B, and C, bottom right, yielded $R_{wp} = 22.5\%$ and $\chi^2 = 0.103$.

The local structure obtained from the pair distribution analysis clearly differs from the average order as seen by diffraction because of nonrandom distribution of the $[Fe^{II}(CN)_6]^{4-}$ vacancies in the Prussian blue pigments. The lattice parameters and interatomic bond distances resulting from the pair distribution analyses of **3**, **4**, **7**, and **8** are given in Table 6, and the corresponding A, B, and C phase percentages are given in Table 7. The observed phase percentages confirm that the distribution of structural vacancies in the soluble Prussian blue pigments is similar to those in the insoluble Prussian blue pigments. Thus, short-range order in a Prussian blue pigment is better described by considering several ordered phases than with an average structure, an average structure that is only adequate for describing the long-range order in Prussian blues pigments.

Table 7. Phase Percentages Obtained from the Pair Distribution Analysis

pigment	A, 0 vacancy	B, 1 vacancy	C, 2 vacancies
$KFe^{III}[Fe^{II}(CN)_6]\cdot xH_2O$ (**3**)	9(2)	42(2)	49(2)
$KFe^{III}[Fe^{II}(CN)_6]\cdot xH_2O$ (**4**)	3(2)	38(2)	59(2)
$KFe^{III}[Fe^{II}(CN)_6]\cdot xH_2O$ (**7**)	12(2)	43(2)	45(2)
$Fe_4^{III}[Fe^{II}(CN)_6]_3\cdot xH_2O$ (**8**)	13(2)	39(2)	48(2)

The above results show that the commercial pigments **7** and **8** and pigment **3**, whose synthesis included an aging step of 2 h under a nitrogen atmosphere, are comparable in that they exhibit similar Mössbauer spectra and X-ray powder diffraction patterns. In contrast, all of the other pigments, except the well-crystallized pigment **4**, are characterized by a larger iron(III) quadrupole splitting and broader diffraction lines. Are these different features related to the inherent short-range order? In other words, does the distribution of the ordered substructures containing zero, one, or two vacancies significantly change with the method of pigment synthesis? To answer these questions, the pair distribution analysis was also carried out for pigments **3** and **4**, and the results are shown in Figure S11 and given in Tables 6 and 7. The broadening of the pair distribution peaks, which is related to the disorder, clearly differs in these pigments. The degree of disorder can be related to the substructure distribution; see Table 7. Although **3** has a substructure distribution similar to that of commercial pigments **7** and **8**, pigment **4** is characterized by a relatively large percentage of the substructure C, which corresponds to two vacancies. Thus, **4** contains more iron(II) site vacancies than does **3**. The presence of numerous lattice defects can explain the higher strain evidenced by the Williamson–Hall analysis and the larger iron(III) quadrupole splitting observed for **4**. However, the number of vacancies present cannot be directly calculated from the substructure distribution because the nearby unit cells share lattice edges. The final number of vacancies depends on how the three substructures arrange themselves together.

X-ray Absorption Spectroscopy. The X-ray near-edge and extended X-ray absorption fine structure spectra of several Prussian blue pigments have been measured in transmission mode at the DUBBLE Dutch-Belgian beamline BM26 at the ESRF, Grenoble, France. Two major features in the X-ray absorption spectra, shown in Figure 15, are worthy of comment, the main edge and the pre-edge; more detailed analysis is given in the Supporting Information.

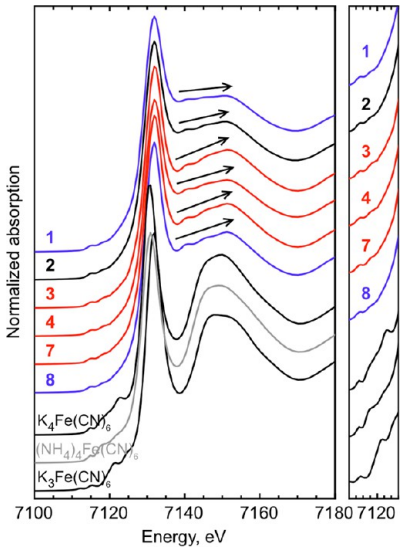

Figure 15. Iron K-edge X-ray absorption spectra of **1**–**4**, **7**, **8**, and three reference compounds.

For all of the pigments, the iron K-edge absorption begins at 7129.30 eV with an accuracy of ±0.26 eV, or one-half the 0.52 eV step per data point. The steepness of the absorption edge is related to the confinement of the final states and the core–hole lifetime. The main edge peak is broadened by both the presence of the two iron oxidation states and their environmental

dx.doi.org/10.1021/jp3111327 | J. Phys. Chem. C 2013, 117, 9693–9712

vacancies. It is worth noting that the contributions of the iron(II) and iron(III) ions to the main edge peak cannot be separated.

The pre-edge is the typically weak absorption found just below the energy of the K-edge. These transitions are related to the local site symmetry and iron electronic configuration[56] and involve linear combinations of molecular orbitals of specific symmetry. Strong pre-edge absorptions are associated with a breaking of the inversion symmetry, and, in the case of centrosymmetric molecules, such as in Prussian blue pigments, the pre-edge absorptions are very weak and result rather from quadrupole transitions.[56]

The X-ray absorption near-edge spectra of all of the Prussian blue pigments studied herein are rather similar, and there is no significant difference between the soluble and insoluble Prussian blues. The different feature that should be noted is the slope, indicated by the arrows in Figure 15 of the absorption just above the main iron K-edge absorption. This feature may be related to a specific vacancy distribution, as evidenced by the pair distribution analysis. Some authors have explained this feature in terms of a distorted Fe^{II}–C–N–-Fe^{III}–N–C–Fe^{II} arrangement and its deviation from linearity.[57]

Both soluble and insoluble Prussian blues exhibit similar extended X-ray absorption spectra in *k*-space and in *R*-space; the spectra for soluble pigment **7** are shown in Figure 16 and are

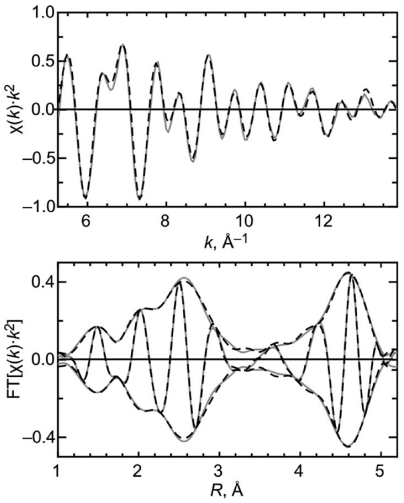

Figure 16. Iron K-edge $\chi(k)\cdot k^2$ and FT$[\chi(k)\cdot k^2]$ spectra with $\Delta k \approx 5.3$–13.9 Å^{-1} and ΔR = 1.0–5.2 Å for soluble pigment **7**. The experimental data, solid line, and the fit, dotted line, agree well.

similar to those previously published[58] for a soluble commercial pigment. This similarity suggests that the incorporation of alkali cations does not appear to significantly modify the coordination environment of the iron ions and supports the revised structural model for soluble Prussian blue pigments proposed herein.

Bond distances, coordination numbers, Debye–Waller factors, and inner potential corrections obtained by fitting the X-ray absorption spectra of **1**–**4**, **7**, and **8** are reported in Table S5. The initial fitting model has been described elsewhere;[14] the Debye–Waller factors, σ^2, and the inner potentials, E_0, are reported relative to those of $K_4Fe(CN)_6$, used as a reference compound, and thus are reported as $\Delta\sigma^2$ and ΔE_0. No significant differences in the X-ray absorption spectra of the insoluble and soluble pigments were observed, and the same model over a *k*-range of ca. 5.3–13.9 Å^{-1} was used; a virtually perfect fit for soluble pigment **7** is shown in Figure 16 and is representative of all of the fits.

The definition of the coordination number, *N*, in the fitting model of the extended X-ray absorption spectra differs from that of the usual coordination number. Because the two iron(II) and iron(III) ions are not differentiated by this technique, only the average iron ionic environment is probed. In one perfect cubic unit cell of either the soluble, **7**, or the insoluble, **8**, Prussian blue pigments, the iron(II) ions have six carbon, six nitrogen, and six iron(III) neighbors in their first, second, and third shells, respectively. Similarly, the iron(III) ions have six nitrogen, six carbon, and six iron(II) neighbors in their first, second, and third shells, respectively. Hence, the average coordination environment of one iron ion is composed of three carbon and three nitrogen, three nitrogen and three carbon, and six iron(II/III) neighbors, in the first, second, and third shells, respectively.

Although all of the Prussian blue pigments exhibit very similar bond distances, the pigments exhibit significantly different refined coordination numbers, *N*, especially in the iron(II)–iron(III) coordination number; see Figure 17. As expected for a

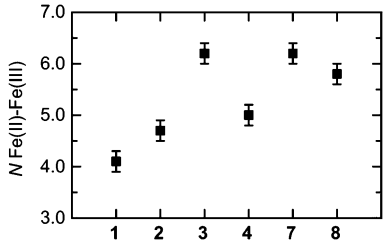

Figure 17. Iron(II)–iron(III) coordination number, *N*, for Prussian blue pigments.

perfect cubic unit cell, pigments **3**, **7**, and **8** all have an iron(II)–iron(III) coordination number of ca. 6; this similarity is expected because the preparation of **3** was based on the synthesis of Prussian blue described in patents and includes an aging time of the Berlin white precipitate under nitrogen as is the case for **7** and **8**. The remaining pigments were synthesized either in ambient atmosphere or without any aging and have smaller iron(II)–iron(III) coordination numbers. This reduction is undoubtedly correlated with the presence of vacancies in the lattice with some local order, as previously observed in the above pair distribution analysis.

Raman Spectral Analysis. The Raman spectra of pigments **3**, **4**, **7**, and **8**, and potassium ferrocyanide, $K_4Fe(CN)_6\cdot 3H_2O$, and potassium ferricyanide, $K_3Fe(CN)_6$, are shown in Figure 18. Because these samples are all cyanides, they all exhibit[59] sharp CN^- stretching scattering, ν(CN), between 2000 and 2200 cm^{-1}. In aqueous solution, the ν(CN) stretching mode for free CN^- anion occurs at 2080 cm^{-1}; ν(CN) is observed to increase upon coordination to a metal cation. For example, the ν(CN) bands are at 2135 and 2130 cm^{-1} in $K_3Fe^{III}(CN)_6$ and at 2082 and 2066 cm^{-1} in $K_4Fe^{II}(CN)_6\cdot 3H_2O$. The difference results because of the differences in the iron oxidation state; the higher is the iron oxidation state, the more effective is the iron cation to CN^- σ-bonding.

The Prussian blue pigments, potassium ferrocyanide, and ferricyanide all crystallize such that many or most of the iron cations experience a local O_h point group symmetry and thus have a local center of symmetry and the two ν(CN) stretching modes are assigned to the A_{1g} and E_g vibrations; only the F_{1u} mode is infrared active, as is stated by the mutual exclusion rule.

dx.doi.org/10.1021/jp3111327 | J. Phys. Chem. C 2013, 117, 9693–9712

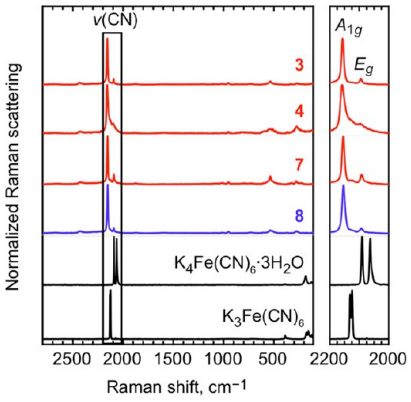

Figure 18. Raman spectra of selected Prussian blue pigments. Each spectrum has been normalized to the intensity of the ν(CN) scattering.

Recent studies[60,61] of the vibrational spectra of the cyanide ligand in Prussian blue analogues indicate that the totally symmetric A_{1g} Raman mode often has both higher energy and intensity.

The Prussian blue pigment Raman scattering in the low-frequency spectral region corresponds to the stretching and bending modes, ν(Fe−C) at 600−350 cm^{-1}, δ(Fe−C−N) at 500−350 cm^{-1}, and δ (C−Fe−C) at 130−60 cm^{-1}.[59,62] However, the assignment of each specific low-frequency band has not been reported in the literature.

To a first approximation, all of the Raman spectra appear to be very similar, see Figure 18, and there does not seem to be any characteristic feature that is correlated with the Prussian blue preparation. By taking into account the experimental error estimated to be ±2 cm^{-1}, the positions of the A_{1g} mode at 2154 cm^{-1} and the E_g mode at 2090 cm^{-1} are all identical and agree with previously reported results.[59,62] It is noteworthy that the ν(CN) scattering is broader in the pigments than in the highly crystalline $K_3Fe^{III}(CN)_6$ and $K_4Fe^{II}(CN)_6{\cdot}3H_2O$. The broadening of the scattering varies slightly in the pigments. For example, **4**, which has been prepared with no aging of the Berlin white precipitate, exhibits broader scattering and a less well-resolved E_g mode. This may be due to poor crystallinity and local disorder in **4** as is evidenced above.

DISCUSSION AND CONCLUSIONS

The objective in this investigation has been the identification of the various compositional, structural, and spectral properties of Prussian blue pigments that vary with their method of synthesis. The longer term goal of the investigation is to use this newly acquired knowledge to better understand how the color of both modern and ancient Prussian blue pigments changes with time and light exposure and how to better conserve painting and related cultural objects that contain Prussian blue pigments.

From the thorough characterization of the modern Prussian blue pigments studied herein, two major features appear to be strongly dependent on the preparative method of the pigments, the particle size and the local disorder. Both features strongly influence the color of the pigment. As a result, well-crystallized Prussian blues, with cubic crystals of ca. 5 μm length, cannot be considered as artist's pigments because they are so poorly colored. Commercial Prussian blues pigments and pigments that were prepared according to an indirect method under a nitrogen atmosphere and with an aging of the Berlin white precipitate exhibit larger pigment particles of ca. 50−80 nm size than do the remaining pigments, which consist of particles smaller than 15 nm. The particle size in the pigments has been directly determined by scanning electron microscopy, and the crystallite size, that is, the coherence length, has been indirectly derived from the reflection broadening in the X-ray powder diffraction patterns. Although the primary particle size does not necessarily correspond to the crystallite size, both crystallites and particles seem to have similar dimensions in the pigments studied.

The Berlin white aging step and the atmosphere during aging have been identified as the most significant factors that affect the particle size. It is well-known that an aging step can help a pigment to tend toward or to reach a longer-term stability. Thermodynamic stability implies a minimization of the surface area of the precipitate. Therefore, an aging of colloidal suspension, as is observed herein, usually tends to increase the particle size and stability.[63] As is evidenced by X-ray powder diffraction, Prussian blue pigments that have been aged during synthesis are indeed more crystalline and exhibit sharper reflections. Crystal growth and aging time are thus directly correlated. However, the crystal growth is less significant when the aging step occurs in the ambient air atmosphere because the oxygen in air rapidly oxidizes the Berlin white precipitate into Prussian blue and no further crystallite growth and stabilization then occurs.

Results obtained by iron K-edge X-ray absorption spectroscopy, pair distribution analysis, and iron-57 Mössbauer spectroscopy indicate a local disorder in all of the Prussian blue pigments. This inherent structural disorder, which is representative of the entire class of cubic polynuclear transition-metal cyanide complexes, is well-known.[12] This is the reason the structures of Prussian blues and related transition-metal cyanides are usually approximated by the *Fm*3*m* space group. However, the Rietveld refinement of X-ray powder diffraction results always using a cubic primitive *Pm*3*m* model, as has been clearly demonstrated herein, permits an evaluation of the degree of ordering by means of the occupancy parameter, *p*, in both soluble and insoluble Prussian blues. The soluble potassium cation containing Prussian blue structure has been revisited, and it can be described with the *Pm*3*m* space group where approximately one-quarter of the $[Fe(CN)_6]^{4-}$ anion sites are vacant. The structural similarity between the insoluble and soluble Prussian blues may explain why the iron-57 Mössbauer spectra and the iron K-edge absorption spectra of both insoluble and soluble Prussian blue are so similar.

The local short-range disorder observed in Prussian blue pigments by pair distribution analysis can be quantified by considering three different ordered substructures. The probability of having a unit cell containing more than one vacancy increases for the poorly crystallized Prussian blue pigments. As a result, the number of Fe^{II}−CN−Fe^{III} pathways is decreasing, as revealed by iron K-edge X-ray absorption studies. Consequently, highly disordered Prussian blue pigments are less intensely blue because the probability of intervalent electron transfer is weakened. Because the small particle size results from a rapid crystallization, the presence of additional defects in the lattice is also expected.

In conclusion, the preparation methods of Prussian blue determine the permanence of Prussian blue in paint layers. If not prepared to optimize particle size, the pigment will contain small particles that will tend to fade more rapidly upon light exposure than larger particles because of their increased surface area.[18] Further, the presence of $[Fe(CN)_6]^{4-}$ vacancies in the Prussian blue pigment is also expected to play a key role in the degradation mechanism in paint layers because of increased interaction

dx.doi.org/10.1021/jp3111327 | J. Phys. Chem. C 2013, 117, 9693−9712

between the medium and the admixed pigment, as was recently reported.[20]

■ ASSOCIATED CONTENT

Supporting Information

Synthetic information, spectral reflectance and absorbance of paint layers containing Prussian blue and titanium white, optical photomicrograph of a Prussian blue pigment, iron-57 Mössbauer spectral results on various Prussian blue pigments, thermogravimetric and differential scanning calorimetry of several Prussian blue pigments, experimental information and results of particle induced X-ray emission spectral analysis, background information and application of the Scherrer and Williamson−Hall methods to Prussian blue pigments, extraction and fitting procedure for the pair distribution analysis of the pigment short-range order, and detailed results of the X-ray near-edge absorption spectral analysis. This material is available free of charge via the Internet at http://pubs.acs.org.

■ AUTHOR INFORMATION

Corresponding Author

*Tel.: +32 4 3663696. Fax: +32 4 3662884. E-mail: louise.samain@ulg.ac.be.

Present Address

[⊥]Department of Materials and Environmental Chemistry, Stockholm University, Svante Arrhenius väg 16C, SE-106 91 Stockholm, Sweden.

Notes

The authors declare no competing financial interest.

■ ACKNOWLEDGMENTS

We thank Drs. Geert Silversmit and Bart Vekemans for their help with the measurements on BM26, Drs. Raphaël Hermann and Moulay T. Sougrati for help in measuring some of the Mössbauer spectra, and Dr. Frédéric Hatert for help in recording the X-ray powder diffraction patterns. We also thank Prof. Bernard Gilbert for his support for Raman spectroscopy measurements. We gratefully acknowledge the Fonds National de la Recherche Scientifique of Belgium for financial support through grants 9.456595, 1.5.064.05, and FC 78482, SOLEIL for provision of synchrotron radiation facilities, and the ESRF for granting beam time on ID11 and BM26 (proposals EC 763 and 26-01-875).

■ REFERENCES

(1) Neff, V. D. Electrochemical Oxidation and Reduction of Thin Films of Prussian Blue. *J. Electrochem. Soc.* **1978**, *125*, 886−887.

(2) Mortimer, R. J. Electrochromic Materials. *Annu. Rev. Mater. Res.* **1997**, *41*, 147−156.

(3) De Tacconi, N. R.; Rajeshwar, K.; Lezna, R. O. Metal Hexacyanoferrates: Electrosynthesis, in Situ Characterization, and Applications. *Chem. Mater.* **2003**, *15*, 3046−3062.

(4) Verdaguer, M.; Bleuzen, A.; Marvaud, V.; Vaissermann, J.; Seuleiman, M.; Desplanches, C.; Scuiller, A.; Train, C.; Garde, R.; Gelly, G.; et al. Molecules to Build Solids: High TC Molecule-based Magnets by Design and Recent Revival of Cyano Complexes Chemistry. *Coord. Chem. Rev.* **1999**, *190−192*, 1023−1047.

(5) Ito, A.; Suenaga, M.; Ono, K. Mössbauer Study of Soluble Prussian Blue, Insoluble Prussian Blue, and Turnbull's Blue. *J. Chem. Phys.* **1968**, *48*, 3597−3599.

(6) Faustino, P. J.; Yang, Y.; Progar, J. J.; Brownell, C. R.; Sadrieh, N.; May, J. C.; Leutzinger, E.; Place, D. A.; Duffy, E. P.; Houn, F.; et al. Quantitative Determination of Cesium Binding to Ferric Hexacyanoferrate: Prussian Blue. *J. Pharm. Anal.* **2008**, *47*, 114−25.

(7) Pyrasch, M.; Toutianoush, A.; Jin, W.; Schnepf, J.; Tieke, B. Self-assembled Films of Prussian Blue and Analogues: Optical and Electrochemical Properties and Application as Ion-sieving Membranes. *Chem. Mater.* **2003**, *15*, 245−254.

(8) Xidis, A.; Neff, V. D. On the Electronic Conduction in Dry Thin Films of Prussian Blue, Prussian Yellow, and Everitt's Salt. *J. Electrochem. Soc.* **1991**, *138*, 3637−3642.

(9) Wojdel, J. C.; Bromley, S. T. Band Gap Variation in Prussian Blue via Cation-Induced Structural Distortion. *J. Phys. Chem. B* **2006**, *110*, 24294−24298.

(10) Robin, M. B. The Color and Electronic Configurations of Prussian Blue. *Inorg. Chem.* **1962**, *1*, 337−342.

(11) Chadwick, B. M.; Sharpe, A. G. Transition Metal Cyanides and Their Complexes. In *Advances in Inorganic Chemistry and Radiochemistry*; Emeléus, H. J., Sharpe, A. G., Eds.; Academic Press: New York and London, 1966; Vol. *8*, p 83.

(12) Ludi, A. In *Mixed-Valence Compounds: Theory and Applications in Chemistry, Physics, Geology, and Biology*; Brown, D. B., Ed.; Springer: New York, 1979; Vol. *58*, p 25.

(13) Kirby, J.; Saunders, D. Fading and Colour Change of Prussian Blue: Methods of Manufacture and the Influence of Extenders. *Natl. Gallery Technical Bull.* **2004**, *25*, 73−99.

(14) Samain, L.; Silversmit, G.; Sanyova, J.; Vekemans, B.; Salomon, H.; Gilbert, B.; Grandjean, F.; Long, G. J.; Hermann, R. P.; Vincze, L.; et al. Fading of Modern Prussian Blue Pigments in Linseed Oil Medium. *J. Anal. At. Spectrom.* **2011**, *26*, 930−941. Typographical errors occurred in Table 3 of this reference. All iron(II) isomer shifts are negative.

(15) Keggin, J. F.; Miles, F. D. Structures and Formulae of the Prussian Blues and Related Compounds. *Nature* **1936**, *137*, 577−578.

(16) Bueno, P. R.; Ferreira, F. F.; Giménez-Romero, D.; Oliveira Setti, G.; Faria, R. C.; Gabrielli, C.; Perrot, H.; Garcia-Jareno, J. J.; Vicente, F. Synchrotron Structural Characterization of Electrochemically Synthesized Hexacyanoferrates Containing K^+: A Revisited Analysis of Electrochemical Redox. *J. Phys. Chem. C* **2008**, *112*, 13264−13271.

(17) Woodward, J. Praeparation Caerulei Prussiaci ex Germania Missa ad Johannem Woodward. *Philos. Trans. R. Soc., A* **1724**, *XXXIII*, 15.

(18) Samain, L.; Grandjean, F.; Long, G. J.; Martinetto, P.; Bordet, P.; Sanyova, J.; Strivay, D. Synthesis and Fading of Eighteenth-century Prussian Blue Pigments: a Combined Study by Spectroscopic and Diffractive Techniques using Laboratory and Synchrotron Radiation Sources. *J. Synchrotron Rad.* **2013**, *20*, 460−473.

(19) Krafft, S. Pour l'emploi d'une nouvelle substance propre à fabriquer le bleu de Prusse. *Description des machines et procédés pour lesquels des brevets d'invention ont été pris sous le régime de la loi du 5 juillet 1844*; Paris, 1854; Vol. *17*, pp 159−160.

(20) Samain, L.; Gilbert, B.; Grandjean, F.; Long, G. J.; Strivay, D. Redox Reactions in Prussian Blue Containing Paint Layers as a Result of Light Exposure. *J. Anal. At. Spectrom.* **2013**, *28*, 524−535.

(21) Maer, K., Jr.; Beasley, M. L.; Collins, R. L.; Milligan, W. O. Structure of the Titanium-iron Cyanide Complexes. *J. Am. Chem. Soc.* **1968**, *90*, 3201−3208.

(22) Delamare, F. *Bleus en Poudres, de l'Art à l'Industrie, 5000 Ans d'Innovations*; Ecole des Mines de Paris: Paris, 2007; p 231.

(23) Buser, H.; Schwarzenbach, D.; Petter, W.; Ludi, A. The Crystal Structure of Prussian Blue: $Fe_4[Fe(CN)_6]_3 \cdot xH_2O$. *Inorg. Chem.* **1977**, *16*, 2704−2710.

(24) Samain, L. Degradation Mechanisms of Prussian Blue Pigments in Paint Layers. Ph.D. Thesis, University of Liège, March 2012.

(25) Weber, G.; Martinot, L.; Strivay, D.; Garnir, H.-P.; George, P. Application of PIXE and PIGE under Variable Ion Beam Incident Angle to Several Fields of Archaeometry. *X-Ray Spectrom.* **2005**, *34*, 297−300.

(26) Weatherstone, A.; Vormwald, M.; Boyd, N.; Campbell, I. *The GUPIXWIN Manual and User Guide*; University of Guelph, 2000.

(27) Hammersley, A. P.; Svensson, S. O.; Hanfland, M.; Fitch, A. N.; Haüsermann, D. Two-dimensional Detector Software: From Real Detector to Idealised Image or Two-theta Scan. *J. High Pressure Res.* **1996**, *14*, 235−248.

(28) Proffen, T.; Billinge, S. J. L. PDFFIT, a Program for Full Profile Structural Refinement of the Atomic Pair Distribution Function. *J. Appl. Crystallogr.* **1999**, *32*, 572−575.
(29) Qiu, X.; Thompson, J. W.; Billinge, S. J. L. PDFgetX2: a GUI Driven Program to Obtain the Pair Distribution Function from X-ray Powder Diffraction Data. *J. Appl. Crystallogr.* **2004**, *37*, 678−678.
(30) Farrow, C. L.; Juhas, P.; Liu, J. W.; Bryndin, D.; Bozin, E. S.; Bloch, J.; Proffen, T.; Billinge, S. J. L. PDFfit2 and PDFgui: Computer Programs for Studying Nanostructure in Crystals. *J. Phys.: Condens. Matter* **2007**, *19*, 335219.
(31) Rodriguez-Carvajal, J. Recent Advances in Magnetic Structure Determination by Neutron Powder Diffraction. *Physica B* **1993**, *192*, 55−69.
(32) Silversmit, G.; Poelman, H.; Balcaen, V.; Heynderickx, P. M.; Olea, M.; Nikitenko, S.; Bras, W.; Smet, P. F.; Poelman, D.; De Gryse, R.; et al. In-situ XAS study on the Cu and Ce Local Structural Changes in a CuO-CeO_2/Al_2O_3 Catalyst under Propane Reduction and Re-oxidation. *J. Phys. Chem. Solids* **2009**, *70*, 1274−1284.
(33) Vaarkamp, M.; Linders, J. C.; Koningsberger, D. C. A New Method for Parameterization of Phase Shift and Backscattering Amplitude. *Physica B* **1995**, *208−209*, 159−160.
(34) Vaarkamp, M.; Dring, I.; Oldman, R. J.; Stern, E. A.; Koningsberger, D. C. Comparison of Theoretical Methods for the Calculation of Extended X-ray-Absorption Fine Structure. *Phys. Rev. B* **1994**, *50*, 7872−7883.
(35) Cook, J. W., Jr.; Sayers, D. Criteria for Automatic X-ray Absorption Fine Structure Background Removal. *J. Appl. Phys.* **1981**, *52*, 5024−5031.
(36) Koningsberger, D. C.; Mojet, B.; van Dorssen, G.; Ramaker, D. XAFS Spectroscopy; Fundamental Principle and Data Analysis. *Top. Catal.* **2000**, *10*, 143−145.
(37) Ankudinov, A.; Ravel, B.; Rehr, J.; Conradson, S. Real-space multiple-scattering calculation and interpretation of X-ray-absorption near-edge structure. *Phys. Rev. B* **1998**, *58*, 7565−7576.
(38) Oyarzùn, J. M. *Pigment Processing, Physico-chemical Principles*; Vincentz Verlag: Hannover, 2000.
(39) Buxbaum, G.; Pfaff, G. *Industrial Inorganic Pigments*, 3rd ed.; Wiley-VCH Verlag: Weinheim, 2005.
(40) Rosseinsky, D. R.; Lim, H.; Jiang, H. J.; Chai, J. W. Optical Charge-transfer in Iron(III) Hexacyanoferrate(II): Electro-intercalated Cations Induce Lattice-energy-dependent Ground-State Energies. *Inorg. Chem.* **2003**, *42*, 6015−6023.
(41) Gratzfeld, E.; Clausen, E.; Reinhardt, H.; Schaefer, H. Iron Blue Pigment, Process for Making the Same and Use. U.S. Patent 4,378,995, April 5, 1983.
(42) Kaye, S. S.; Long, J. R. The Role of Vacancies in the Hydrogen Storage Properties of Prussian Blue Analogues. *Catal. Today* **2007**, *120*, 311−316.
(43) Kubelka, P.; Munk, F. Ein Beitrag zur Optik der Farbanstriche. *Z. Tech. Phys.* **1931**, *12*, 593−601.
(44) Mie, G. Beiträge zur Optik trüber Medien, Speziell Kolloidaler Metallösungen. *Ann. Phys.* **1908**, *330*, 377−445.
(45) Taft, W. S.; Mayer, J. W. *The Science of Paintings*; Springer: New York, 2000.
(46) Wertheim, G. K.; Rosencwaig, A. Characterization of Inequivalent Iron Sites in Prussian Blue by Photoelectron Spectroscopy. *J. Chem. Phys.* **1971**, *54*, 3235−3237.
(47) Fluck, E.; Inoue, H.; Yanagisawa, S. Mössbauer and X-ray Photoelectron Spectroscopic Studies of Prussian Blue and its Related Compounds. *Z. Anorg. Allg. Chem.* **1977**, *430*, 241−249.
(48) Grandjean, F.; Long, G. J.; Samain, L. The Pivotal Role of Mössbauer Spectroscopy in the Characterization of Prussian Blue and Related Iron Cyanide Complexes. *Mössbauer Effect Research Data J.* **2012**, *35*, 143−153.
(49) Shenoy, G. K.; Wagner, F. E.; Kalvius, G. M. In *Mössbauer Isomer Shifts*; Shenoy, G. K., Wagner, F. E., Eds.; North-Holland: Amsterdam, 1978; p 49.
(50) Owen, T.; Grandjean, F.; Long, G. J.; Domasevitch, K. V.; Gerasimchuk, N. N. Synthesis and Characterization of Two Intensely Colored Tris(benzoylcyanoxime)iron(II) Anionic Complexes. *Inorg. Chem.* **2008**, *47*, 8704−8713.
(51) Ware, M. Prussian Blue: Artists' Pigment and Chemists' Sponge. *J. Chem. Educ.* **2008**, *85*, 612−620.
(52) Guinebretière, R. *Diffraction des Rayons X sur Echantillons Polycristallins, Instrumentation et Etude de la Microstructure*; Hermes Science and Lavoisier: Paris, 2006.
(53) Williamson, G. K.; Hall, W. H. X-ray Line Broadening from Filed Aluminium and Wolfram. *Acta Metall.* **1953**, *1*, 22−31.
(54) Rietveld, H. M. Line Profiles of Neutron Powder-diffraction Peaks for Structure Refinement. *Acta Crystallogr.* **1967**, *22*, 151−152.
(55) Herren, F.; Fischer, P.; Ludi, A.; Haelg, W. Neutron Diffraction Study of Prussian Blue, $Fe_4[Fe(CN)_6]_3 \cdot xH_2O$. Location of Water Molecules and Long-range Magnetic Order. *Inorg. Chem.* **1980**, *19*, 956−959.
(56) Bunker, G. *Introduction to XAFS, A Practical Guide to X-ray Absorption Fine Structure Spectroscopy*; Cambridge University Press: Cambridge, UK, 2010.
(57) Kulesza, P. J.; Zamponi, S.; Berrettoni, M.; Marassi, R.; Malik, M. A. Preparation, Spectroscopic Characterization and Electrochemical Charging of the Sodium-containing Analogue of Prussian Blue. *Electrochim. Acta* **1995**, *40*, 681−688.
(58) Glatzel, P.; Jacquamet, L.; Bergmann, U.; de Groot, M. F. M.; Cramer, S. P. Site-Selective EXAFS in Mixed-Valence Compounds Using High-Resolution Fluorescence Detection: A Study of Iron in Prussian Blue. *Inorg. Chem.* **2002**, *41*, 3121−3127.
(59) Nakamoto, K. *Infrared and Raman Spectra of Inorganic and Coordination Compounds*; Wiley-Interscience Publication: New York, 1978; p 178.
(60) Kettle, S. F. A.; Aschero, G. L.; Diana, E.; Rossetti, R.; Stanghellini, P. L. The Vibrational Spectra of the Cyanide Ligand Revisited: Terminal Cyanides. *Inorg. Chem.* **2006**, *45*, 4928−4937.
(61) Kettle, S. F. A.; Diana, E.; Marchese, E. M. C.; Boccaleri, E.; Stanghellini, P. L. The Vibrational Spectra of the Cyanide Ligand Revisited: the ν(CN) Infrared and Raman Spectroscopy of Prussian Blue and its Analogues. *J. Raman Spectrosc.* **2011**, *42*, 2006−2014.
(62) Barsan, M. M.; Butler, I. S.; Fitzpatrick, J.; Gilson, D. F. R. High-pressure Studies of the Micro-Raman Spectra of Iron Cyanide Complexes: Prussian Blue ($Fe_4[Fe(CN)_6]_3$), Potassium Ferricyanide ($K_3[Fe(CN)_6]$), and Sodium Nitroprusside ($Na_2[Fe(CN)_5(NO)] \cdot 2H_2O$). *J. Raman Spectrosc.* **2011**, *42*, 1820−1824.
(63) Jolivet, J. P.; Henry, M.; Livage, J. *Metal Oxide Chemistry and Synthesis: From Solution to Solid State*; John Wiley & Sons: Chichester, 2000; pp 39−40.